

Pair production in low luminosity galactic nuclei

Monika Mościbrodzka¹, Charles F. Gammie^{1,2}, Joshua C. Dolence²,
Hotaka Shiokawa²

¹ *Department of Physics, University of Illinois, 1110 West Green Street, Urbana, IL 61801*

² *Astronomy Department, University of Illinois, 1002 West Green Street, Urbana, IL 61801*

mmosc@illinois.edu

ABSTRACT

Electron-positron pairs may be produced near accreting black holes by a variety of physical processes, and the resulting pair plasma may be accelerated and collimated into a relativistic jet. Here we use a self-consistent dynamical and radiative model to investigate pair production by $\gamma\gamma$ collisions in weakly radiative accretion flows around a black hole of mass M and accretion rate \dot{M} . Our flow model is drawn from general relativistic magnetohydrodynamic simulations, and our radiation field is computed by a Monte Carlo transport scheme assuming the electron distribution function is thermal. We argue that the pair production rate scales as $r^{-6}M^{-1}\dot{M}^6$. We confirm this numerically and calibrate the scaling relation. This relation is self-consistent in a wedge in M, \dot{M} parameter space. If \dot{M} is too low the implied pair density over the poles of the black hole is below the Goldreich-Julian density and $\gamma\gamma$ pair production is relatively unimportant; if \dot{M} is too high the models are radiatively efficient. We also argue that for a power-law spectrum the pair production rate should scale with the observables $L_X \equiv$ X-ray luminosity and M as $L_X^2 M^{-4}$. We confirm this numerically and argue that this relation likely holds even for radiatively efficient flows. The pair production rates are sensitive to black hole spin and to the ion-electron temperature ratio which are fixed in this exploratory calculation. We finish with a brief discussion of the implications for Sgr A* and M87.

Subject headings: accretion, accretion disks — black hole physics — MHD — radiative transfer — Galaxy: center

1. Introduction

Models of zero-obliquity black hole accretion—in which the accretion flow angular momentum is parallel to the black hole spin—typically exhibit a low density “funnel” over

the poles of the black hole. The funnel is empty because the funnel plasma is free to fall into the hole or be ejected to large radius. Magnetic fields do not prevent this: in magnetohydrodynamic (MHD) simulations of radiatively inefficient accretion flows (RIAFs) the funnel magnetic field typically runs in a smooth spiral from the event horizon to large radius (De Villiers et al. 2003; McKinney & Gammie 2004; Komissarov 2005; Hawley & Krolik 2006; Beckwith et al. 2008). Because the field lines do not leave the funnel there is no way for the disk plasma to resupply the funnel plasma.

What process, then, populates the funnel with plasma? And what controls the temperature (or distribution function) of the funnel plasma? These questions bear directly on two interesting problems in black hole jet theory: are jets made of pairs or an electron-ion plasma? And which is more luminous: the base of the jet or the accretion flow? The purpose of this paper is to investigate these questions in the specific context of hot, underluminous accretion flows where nearly *ab initio* models are computationally feasible.

There are several pair creation processes that might populate the funnel with plasma. Plasma close to the event horizon in a RIAF is relativistically hot, and thus can form electron-positron pairs e^\pm through particle-particle (ee , ep), particle-photon ($e\gamma$, $p\gamma$), or photon-photon collisions ($\gamma\gamma$). The cross section near the e^\pm energy threshold is largest for $\gamma\gamma$ interactions, which have a cross section $\sim \sigma_T \equiv$, the Thomson cross section. In the funnel the photon density vastly exceeds the particle density, so $\gamma\gamma$ collisions dominate e^\pm production (Stepney & Guilbert 1983, Phinney 1983, Phinney 1995, Krolik 1999). Pair production by these processes is discussed in e.g. Kusunose & Mineshige 1996 and Esin 1999 in the context of Advection Dominated Accretion Flows (ADAFs, Narayan & Yi 1994). These works, however, focus on the energetic role of pairs in ADAF disks rather than the population and dynamics of pairs in the funnel.

Other processes are important when the density is below the Goldreich & Julian (1969) charge density. Then the plasma can have $\mathbf{E} \cdot \mathbf{B} \neq 0$, and the electric field can directly accelerate particles to high Lorentz factors. The energetic particles Compton upscatter background photons that collide with other background photons and produce a shower of pairs in a pair-photon cascade (Blandford & Znajek 1977; Phinney 1983; Beskin et al. 1992; Hirotani & Okamoto 1998, and recently Vincent & Lebohec 2010).

In this paper we model production of an e^\pm plasma by photon-photon collisions in the funnel above a hot, underluminous accretion disk. At low accretion rates \dot{M} ($\lesssim \dot{M}_{crit} \sim 10^{-6} L_{Edd}/(0.1c^2)$, where $L_{Edd} \equiv$ Eddington luminosity) the disk cools on a timescale longer than the accretion timescale; it is a RIAF. In this regime the radiative and dynamical evolution are decoupled and it is practical to treat both on a nearly *ab initio* basis. Throughout the range of \dot{M} we consider the funnel pair plasma is tenuous enough that annihilation is

negligible, so pair production will be balanced by advective losses such as accretion into the black hole or loss in a wind.

We draw our RIAF model from two and three dimensional general relativistic magnetohydrodynamics simulations (GRMHD, using the HARM code, Gammie et al. 2003; Noble et al. 2009) of an accreting, magnetized torus with zero cooling. The radiation field is calculated as a post-processing step using a Monte Carlo method (`grmonty`, Dolence et al. 2009), and pair production rates are estimated from snapshots of the radiation field using a procedure described in detail below.

This paper is organized as follows. In § 2 we describe the basic model for accretion flow dynamics and radiative transfer. In § 3 we write down the pair production model and present a test problem for our Monte Carlo scheme. Scaling formulas are presented in § 4. In § 5 we show results for a range of black hole masses and accretion rates. We briefly discuss implications for Sgr A* and M87 in § 6 and summarize in § 7.

2. Accretion flow model

We use a numerical model for the accretion flow and for the radiation field; together these nearly *ab initio* models form a numerical laboratory for investigating physical processes near a black hole in a self-consistent way.

2.1. Dynamical model

We use a relativistic MHD model for the accreting plasma (see e.g., Gammie et al. 2003). The initial condition is an equilibrium torus (Fishbone & Moncrief 1976) in orbit around a Kerr black hole with $a_* = 0.94$, where a_*GM^2/c is the hole angular momentum. The torus is seeded with poloidal, concentric loops of weak magnetic field that are parallel to density contours. Small perturbations are added to the internal energy and this seeds the magnetorotational instability, which leads to the development of MHD turbulence in the disk and accretion onto the central black hole. The model extends from slightly inside the event horizon to $r = 40GM/c^2$.

We solve the evolution equations until a quasi-equilibrium accretion flow is established, meaning that the mean structure of the flow is not evolving on the dynamical timescale. Our (untested) hypothesis is that at $r < 15GM/c^2$ the model accurately represent the inner portions of a relaxed accretion flow extending over many decades in radius.

A few of the physical assumptions in the GRMHD model are worth stating explicitly. The equation of state is

$$p = (\gamma_{ad} - 1)u \quad (1)$$

where $\gamma_{ad} = 13/9$ (appropriate for ion temperature $T_i < m_p c^2/k = 1.1 \times 10^{13} K$ and electron temperature $T_e > m_e c^2/k = 5.9 \times 10^9 K$), $p \equiv$ pressure, and $u \equiv$ internal energy density. Particle number is also conserved:

$$(\rho_0 u^\mu)_{;\mu} = 0, \quad (2)$$

where $\rho_0 \equiv$ rest-mass density and $u^\mu \equiv$ four-velocity, in the dynamical evolution. That is, pair production is not included in the dynamical model. The model is therefore consistent only if pair creation is weak enough not to alter the flow dynamics or energetics.

We evolve the GRMHD equations using the `harm` code (Gammie et al. 2003; Noble et al. 2009). `harm` is a conservative scheme that evolves the total energy rather than internal energy of the flow. The MHD equation integration is performed on a uniform grid in modified Kerr-Schild coordinates (Gammie et al. 2003). The coordinates are logarithmic in Kerr-Schild radius r and nonuniform in Kerr-Schild colatitude θ (Boyer-Lindquist and Kerr-Schild r and θ are identical), with zones concentrated toward the midplane of the accretion disk. The inner and outer radial boundaries use outflow boundary conditions. The axisymmetric models use a 256×256 grid, and the single 3D run uses a $192 \times 192 \times 128$ grid. For details of the numerical method, the initial setup and the flow evolution in 2D see Gammie et al. (2003) and McKinney & Gammie (2004). A snapshot of the density, temperature, and magnetic field strength from one of our runs is shown in Figure 1.

2.2. Radiative model

Our radiative model is identical to that applied by Mościbrodzka et al. (2009) to Sgr A*, although here we restrict attention to a thermal plasma with $T_e = T_i$ (except in one case noted below). Synchrotron emission and absorption are included, as is Compton scattering.

Bremsstrahlung is not important in the inner parts of the accretion flow. For a thermal plasma with $\Theta_e \equiv kT_e/(m_e c^2) > 1$ the ratio (synchrotron / bremsstrahlung) cooling $\sim \Theta_e^2/(\alpha\beta)$, where $\alpha \equiv$ fine structure constant and $\beta \equiv 8\pi p/B^2$. At the radii of interest here $\Theta_e \sim 1 - 10^2$, and $\beta \sim 10$, so in an energetic sense synchrotron dominates the direct production of photons.

Synchrotron emission occurs at a characteristic frequency $\nu_s \sim (eB/(2\pi m_e c))\Theta_e^2$ which

is $\ll m_e c^2/h$ for any astrophysically reasonable combination of M and \dot{M} ¹. Potentially pair-producing photons must therefore be produced by Compton scattering.

We compute the radiation field using the general relativistic Monte Carlo radiative transfer code `grmonty` (Dolence et al. 2009). The radiation field is represented by photon packets (photon rays or “superphotons”). Each superphoton is characterized by a weight w = number of physical photons/superphoton, and a wave four-vector k^μ . Superphotons are produced by sampling the emissivity. The wavevector is transported according to the geodesic equation. Along a geodesic w is decremented to account for synchrotron absorption. Compton scattering is incorporated by sampling scattering events. When a superphoton scatters it is divided into a scattered piece with new wavevector k'^μ and new weight w' , and an unscattered piece along the original wavevector with weight $w - w'$. The distribution of scattered k'^μ is consistent with the full Klein-Nishina differential cross section.

We use a “fast light” approximation in treating the radiative transfer. The data from a single time slice t_n (e.g. $\rho_0(t_n, x^1, x^2, x^3)$) is used to calculate the emergent radiation field as if the data, and therefore photon field, were time-independent. We have checked the fast light model against a time-dependent radiative transfer model (Dolence et al. 2010) and verified that this approximation does not introduce significant errors.

2.3. Model scaling

The properties of the accretion flow model are independent of the absolute value of the density (provided the magnetic field strength is scaled appropriately), but the radiative model is not. To scale the model we specify the length unit

$$\mathcal{L} \equiv \frac{GM}{c^2}, \quad (4)$$

¹For the synchrotron emissivity we use the approximate expression of Leung et al. (2010)

$$j_\nu = \frac{\sqrt{2}\pi e^2 n_e \nu_s}{3cK_2(\Theta_e^{-1})} (X^{1/2} + 2^{11/12} X^{1/6})^2 \exp(-X^{1/3}) \quad (3)$$

where $X = \nu/\nu_s$, $\nu_s = 2/9(eB/2\pi m_e c)\Theta_e^2 \sin\theta$ is the synchrotron frequency, θ is an angle between the magnetic field vector and emitted photon, and K_2 is a modified Bessel function of the second kind. The fractional error for this approximate formula is smaller than 1% for $\Theta_e \geq 1$ (where most of the emission occurs) and increases to 10% and more at low frequencies for $\Theta_e \leq 1$ (where there is very little emission). The synchrotron emissivity function peaks at $\nu \approx 8\nu_s$.

time unit

$$\mathcal{T} \equiv \frac{GM}{c^3}, \quad (5)$$

and mass unit \mathcal{M} , which is proportional to the mass accretion rate. M does not set a mass scale because it appears only in the combination GM . Since $\mathcal{M} \lll M$ the accretion flow does not affect the gravitational field.

Given M and \mathcal{M} the radiative transfer calculation is well posed. Typically M can be estimated directly from observations, while \mathcal{M} is varied until the model submillimeter flux matches the observed flux.

2.4. Model limitations

An important limitation of our model is that it treats accreting plasma as a nonradiating ideal fluid. This implies that electrons and ions have an isotropic, thermal distribution function. The potentially important effects of pressure anisotropy and conduction (e.g. Sharma et al. 2006, Johnson & Quataert 2007) are therefore neglected, as are the radiative effects of a nonthermal component in the electron distribution function.

Cooling is also neglected. This is a good approximation in low accretion rate systems like Sgr A*, but a poor approximation in higher accretion rate systems like M87. If one were to turn on cooling but hold the synchrotron flux fixed the density and magnetic field strength (i.e. the mass unit \mathcal{M}) would increase.

3. Pair production

3.1. Basic equations

For a population of photons with distribution function $dN_\gamma/d^3x d^3k$ (here $d^3k \equiv dk_1 dk_2 dk_3$ and 1, 2, 3 are the spatial coordinates) the invariant pair production rate per unit volume is

$$\dot{n}_\pm \equiv \frac{1}{\sqrt{-g}} \frac{dN_\pm}{d^3x dt} = \frac{1}{2} \int \frac{d^3k}{\sqrt{-g} k^t} \frac{d^3k'}{\sqrt{-g} k'^t} \frac{dN_\gamma}{d^3x d^3k} \frac{dN_\gamma}{d^3x d^3k'} \epsilon_{[CM]}^2 \sigma_{\gamma\gamma} c \quad (6)$$

where g is the determinant of $g_{\mu\nu}$, and the factor of 1/2 prevents double-counting. Here $\sigma_{\gamma\gamma}$ is the cross section for $\gamma + \gamma \rightarrow e^+ + e^-$:

$$\frac{\sigma_{\gamma\gamma}}{\sigma_T} = \frac{3}{8 \epsilon_{[CM]}^6} \left[(2 \epsilon_{[CM]}^4 + 2 \epsilon_{[CM]}^2 - 1) \cosh^{-1} \epsilon_{[CM]} - \epsilon_{[CM]} (\epsilon_{[CM]}^2 + 1) \sqrt{\epsilon_{[CM]}^2 - 1} \right] \quad (7)$$

(Breit & Wheeler 1936),

$$\epsilon_{[CM]} = -u_{CM\mu}k^\mu = -u_{[CM]\mu}k'^\mu = \left(\frac{-k_\mu k'^\mu}{2}\right)^{1/2} \quad (8)$$

is the energy of either photon in the center of momentum ([CM]) frame of the two photons, and $u_{[CM]}$ is the four-velocity of the [CM] frame.

Equation 6 is coordinate invariant since $\sqrt{-g}d^3xdt$ is invariant, the distribution function is invariant (because $d^3x d^3k$ is invariant), $\epsilon_{[CM]}$ is a scalar, the cross section is invariant, and $d^3k/\sqrt{-g}k^t$ is invariant. It reduces to the correct rate (cf. eq. 12.7 of Landau & Lifshitz, Classical Theory of Fields) in Minkowski space, and is therefore the correct general expression for the pair production rate. Because \dot{n}_\pm itself is invariant it also describes the pair creation rate in the fluid frame.

We will need the rate of four-momentum transfer from the radiation field to the plasma via pair creation:

$$G^\mu \equiv \frac{1}{\sqrt{-g}} \frac{dP_\pm^\mu}{d^3xdt} = A \frac{1}{2} \int \frac{d^3k}{\sqrt{-g}k^t} \frac{d^3k'}{\sqrt{-g}k'^t} \frac{dN_\gamma}{d^3x d^3k} \frac{dN_\gamma}{d^3x d^3k'} (k^\mu + k'^\mu) \epsilon_{[CM]}^2 \sigma_{\gamma\gamma} c. \quad (9)$$

Here A is a constant that makes the equation dimensionally correct.

3.2. Monte Carlo estimate of pair creation rate

We estimate the integrals (6) and (9) using a Monte Carlo scheme. Given a sample of photons on a time slice t within a small three-volume Δ^3x , a naive estimate is

$$\frac{1}{\sqrt{-g}} \frac{dN_\pm}{d^3xdt} \approx \frac{1}{2} \sum_{i,j} \left(\frac{w_i}{\Delta^3x}\right) \left(\frac{w_j}{\Delta^3x}\right) \frac{1}{\sqrt{-g}k_i^t} \frac{1}{\sqrt{-g}k_j^t} \epsilon_{[CM]}^2 \sigma_{\gamma\gamma} c. \quad (10)$$

where i and j label superphotons.

If there are N_s superphotons in Δ^3x then there are $O(N_s^2)$ pairs of superphotons and the computational cost of (10) is $O(N_s^2)$. One might hope that the error would scale as $1/\sqrt{N_s^2}$ because there are $O(N_s^2)$ pairs, but this is wrong. There are only N_s independent samples and so the error scales as $1/\sqrt{N_s}$.

We obtain an estimate with accuracy that is the same order as (10) at $O(N_s)$ cost by selecting an unbiased sample of N_s pairs of superphotons and evaluating

$$\frac{1}{\sqrt{-g}} \frac{dN_\pm}{d^3xdt} \approx \frac{1}{2} \frac{N_s}{2} \sum_{i,j} \left(\frac{w_i}{\Delta^3x}\right) \left(\frac{w_j}{\Delta^3x}\right) \frac{1}{\sqrt{-g}k_i^t} \frac{1}{\sqrt{-g}k_j^t} \epsilon_{[CM]}^2 \sigma_{\gamma\gamma} c \quad (11)$$

An identical procedure is used to evaluate G^μ .

3.3. Test problem

Does our Monte Carlo procedure accurately estimate the pair production rate? As a check we evaluate pair production rates near two point sources of $E = 4m_e c^2$ photons. The calculation is done in Minkowski space and Cartesian coordinates (so $\sqrt{-g} = 1$), and the optical depth to pair creation is assumed small. At each point we compare the analytic and numerical result.

The expected pair production rate is given by Equation 6. The energy of two colliding photons in their center-of-momentum frame is a function of the cosine μ of the angle between the rays from the two sources: $\epsilon_{[CM]}^2 = (1/2)(1 - \mu)k^t k'^t$. The photon momentum space distribution is a δ function. The number density of photons $dN_\gamma/d^3x = \dot{N}_\gamma/(4\pi r^2 c)$ at distance r from the source, where each source produces photons at rate \dot{N}_γ .

Figure 2 shows a 2D map of the numerically evaluated pair production rate in the plane of the two sources. Figure 3 shows the analytic and numerical pair production rates along the black contour shown in Figure 2 (upper panel), and their difference (lower panel). The error in the numerical rate is $\propto N_s^{-1/2}$, as demonstrated in Figure 4, where N_s is the number of photon packets emitted by each source. Evidently the Monte Carlo method produces an unbiased, convergent estimate of the pair production rate.

4. RIAF scaling laws

In this section we derive scaling relations for the pair production rate in two cases: (1) M and \dot{M} are known and the flow is radiatively inefficient; (2) the spectrum νL_ν and M are known. In case (1) we can numerically evaluate the pair production rate self-consistently and check it against the scaling relation. In case (2) we can do the same, but we also obtain a method for estimating pair production rates from observations that may also apply to flows that are radiatively efficient.

First consider the pair production rate density at a single point in the flow where the plasma-frame photon spectrum is a power-law with high energy cutoff at $\epsilon = E/(m_e c^2) = \epsilon_{max} \gg 1$:

$$\frac{dn}{dE} = \frac{n_0}{m_e c^2} \epsilon^\alpha e^{-\epsilon/\epsilon_{max}} \quad (12)$$

We evaluated the pair production rate density numerically for this energy distribution. A fit to the result over $-3 < \alpha < 2$ and $10 < \epsilon_{max} < 160$ gives

$$\frac{\dot{n}_\pm}{n_0^2 \sigma_T c} \simeq \frac{1}{16} e^{2\alpha/3} \left(\frac{4}{3} + \epsilon_{max}^{\alpha/2}\right)^4 \ln\left(\frac{\epsilon_{max}}{2}\right) \quad (13)$$

(Zdziarski [1985] gives a similar expression in the $\epsilon_{max} \gg 1$ limit). At worst the fit is ≈ 2 too small for $\alpha \approx 0$ and $\epsilon_{max} = 160$. For $\alpha < -2$, which is typical of our models, the relative error is smaller than 60%.

For $\alpha > 0$ ($d \ln \nu L_\nu / d \ln \nu > 2$) pair production is dominated by photons with $\epsilon \sim \epsilon_{max}$, and \dot{n}_\pm is therefore sensitive to ϵ_{max} . For $\alpha < 0$, pair production is dominated by pairs with $\epsilon \sim 1$ in the center-of-momentum frame. In this case there is an equal contribution from each logarithmic interval in energy in the plasma frame, and the pair production rate density is therefore weakly (logarithmically) dependent on ϵ_{max} .

Our models have $\alpha \lesssim -2$ so \dot{n}_\pm is insensitive to ϵ_{max} . Therefore the effective number density of pair producing photons is $n_0 \sim L_{512} / (4\pi \mathcal{L}^2 m_e c^3)$, where $L_{512} \equiv \nu L_\nu(512 \text{keV})$ and $\dot{n}_\pm \sim n_0^2 \sigma_{TC}$. Then

$$\dot{n}_\pm \simeq \left(\frac{L_{512}}{m_e c^2} \frac{1}{\mathcal{L}^2 c} \right)^2 \sigma_{TC} \times f\left(\frac{r}{\mathcal{L}}, \mu\right). \quad (14)$$

where f is a dimensionless function of Kerr-Schild radius r and colatitude $\theta = \cos^{-1} \mu$.

What do we expect for the spatial distribution of pair production f ? The pair-producing photons are made by upscattering synchrotron photons in a ring of hot gas near the innermost stable circular orbit (ISCO). Away from this ring the density of photons will fall off as $\sim 1/r^2$. The pair production rate also depends on the angle ψ between photon trajectories in the coordinate frame through the geometrical factor $\epsilon_{[CM]}^2 / k_1^t k_2^t \propto 1 - \cos \psi$. At large r $\psi \lesssim 1$ so $1 - \cos \psi \propto 1/r^2$. Then $\dot{n}_\pm \sim r^{-6}$. Compton upscattered photons are also beamed into the plane of the disk by the relativistic orbital motion. If the intensity of photons to be scattered is nearly independent of θ then the pair production rate density should fall off away from the midplane as the density of upscattering electrons $\sim \exp(-\mu^2 / (2\sigma_\rho^2))$ where $\sigma_\rho \simeq 0.3$. Gathering these estimates together we expect $f \sim \exp(-\mu^2 / (2\sigma_\rho m^2)) / r^6$ where $\sigma_\pm \approx \sigma_\rho$.

4.1. Scalings with model parameters

Now suppose we know the mass $M = m_8 M_8$ ($M_8 \equiv 10^8 M_\odot$) and the accretion rate $\dot{M} = \dot{m} \dot{M}_{Edd}$, where $\dot{M}_{Edd} \equiv L_{Edd} / (\epsilon_{ref} c^2)$ and $\epsilon_{ref} = 0.1$ is a reference accretion efficiency. We assume that photons are produced in a low frequency synchrotron peak and then scattered to $\sim 512 \text{keV}$ by n_{sc} Compton scatterings, where n_{sc} is 1 or 2.

For a plasma that is optically thin to synchrotron absorption at peak, the total number of synchrotron photons at the peak frequency produced per unit time is $\dot{N}_{\nu_{peak}} \simeq$

$4\pi\nu_{peak}j_{\nu_{peak}}\mathcal{L}^3/(h\nu_{peak})$, where $j_{\nu_{peak}}$ is the synchrotron emissivity ². The number density of synchrotron photons is then $n_{\nu_{peak}} \simeq \dot{N}_{\nu_{peak}}/(4\pi\mathcal{L}^2c)$.

A fraction $\tau^{n_{sc}}$ of the peak photons are upscattered to 512 keV, where $\tau = \sigma_T n_e \mathcal{L}$ is the Thomson depth of the plasma, so $n_{512} = n_{\nu_{peak}} \tau^{n_{sc}}$. The mean number of Compton scatterings is $n_{sc} = \log(m_e c^2 / h\nu_{peak}) / \log A$, where $A \approx 16\Theta_e^2$ is the photon energy enhancement in single scattering by a relativistic electron, so

$$n_{sc} \simeq a_1 + a_2 \log \frac{m_8}{\dot{m}}. \quad (15)$$

We determine a_1 and a_2 numerically but for a reference model with $\dot{m} = 10^{-8}$ and $m_8 = 4.5 \times 10^{-2}$ (Sgr A*), the average value of $n_{sc} \approx 1 - 2$.

Assuming $\dot{M} \sim 4\pi\rho c\mathcal{L}$, the magnetic pressure is comparable to the gas pressure and both are $\sim \rho c^2$, the plasma density, magnetic field strength, and plasma temperature (close to the virial temperature) scale as

$$n_e \simeq \frac{1}{\epsilon_{ref}} \left(\frac{c^2}{GM_8\sigma_T} \right) \left(\frac{\dot{m}}{m_8} \right) \quad (16)$$

$$\frac{B^2}{8\pi} \simeq \frac{1}{\epsilon_{ref}} \left(\frac{m_p c^4}{GM_8\sigma_T} \right) \left(\frac{\dot{m}}{m_8} \right) \quad (17)$$

and

$$\Theta_e \simeq \frac{1}{30} \frac{m_p}{m_e}. \quad (18)$$

The mean emission Θ_e corresponds to the mean value near the ISCO, and therefore increases with a_* . Combining,

$$\dot{n}_{\pm} \simeq \mathcal{A} \left(\frac{1}{r_0^3 \mathcal{T}} \right) \epsilon_{ref}^{-(2n_{sc}+3)} \alpha_f^2 \frac{m_p}{m_e} \dot{m}^{3+2n_{sc}} f\left(\frac{r}{\mathcal{L}}, \mu\right), \quad (19)$$

where \mathcal{A} is a dimensionless constant to be determined numerically, $r_0 \equiv$ classical electron radius, and $\alpha_f \equiv$ the fine structure constant. From now on unless stated otherwise we will set $\epsilon_{ref} = 0.1$ and the mean number of scatterings $n_{sc} = 1.5$ (numerical results, below, show $1.4 < n_{sc} < 1.6$ for relevant M, \dot{M}). Then

$$\dot{n}_{\pm} \simeq 9 \times 10^{39} \mathcal{A} m_8^{-1} \dot{m}^6 f\left(\frac{r}{\mathcal{L}}, \mu\right). \quad (20)$$

To estimate the jet kinetic luminosity we need the pair production rate:

$$\dot{N}_{\pm} = \int_{r>r_{hor}} \sqrt{-g} d^3x \dot{n}_{\pm} \quad (21)$$

² $j_{\nu_{peak}} \simeq 8\sqrt{2}e^3 n_e B / (27m_e c^2)$, see Leung et al. 2010

where r_{hor} is the horizon radius. Then

$$\dot{N}_{\pm} \simeq \dot{n}_{\pm} \mathcal{L}^3 \simeq 10^{78} \mathcal{A} \dot{m}^{3+2n_{sc}} m_8^2 \text{ s}^{-1} \quad (22)$$

Only pairs made inside the funnel and at $r > r_{st} \equiv$ stagnation radius can escape to large radius (they are “free pairs”); those made at smaller radius or inside the accretion flow are advected into the hole. The free pair fraction is therefore a small multiple of (22).

Evidently the pair production rate density is sensitive to the mass accretion rate, $\dot{n}_{\pm} \sim \dot{m}^6$. This steep dependence shuts off pair production at low accretion rates, making it difficult for low \dot{m} systems like Sgr A* to populate their funnel with pairs. Below we will show that the implied funnel pair density for Sgr A* falls below the Goldreich-Julian charge density (see §5.4).

4.2. Scalings with observables

Assume that from observations we know M , the X-ray luminosity $L_X \equiv l_X L_{\odot}$ (assuming isotropic emission), and the spectral index $\alpha = d \log(\nu L_{\nu}) / d \log \nu$.³ Self-consistent models then permit us to calibrate the relation between these quantities and the pair production rate density. Since this relation depends only on the distribution of pair-producing photons within the source, it seems likely that it can be applied to sources with $\dot{M} > \dot{M}_{crit}$, in which cooling is important.

If the spectrum is power-law from the keV to MeV energy,

$$L_{512}(L_X) \approx L_X e^{4.92\alpha}, \quad (23)$$

$$\dot{n}_{\pm} \approx \mathcal{B} \left(\frac{c^3 \sigma_T L_{\odot}^2}{m_e^2 G^4 M_8^4} \right) l_X^2 e^{(9.26\alpha)} m_8^{-4} f\left(\frac{r}{\mathcal{L}}, \mu\right) \quad (24)$$

where \mathcal{B} is a constant to be determined numerically and $(c^3 \sigma_T L_{\odot}^2 / m_e^2 G^4 M_8^4) \approx 10^{-8} \text{ cm}^{-3} \text{ s}^{-1}$. This assumes that the observed spectrum and the plasma-frame spectrum near the black hole are identical. We checked the plasma-frame spectrum and found it to be a slightly blueshifted version of the observed spectrum; the blueshifting does not change the scaling relation.

The pair production rate is

$$\dot{N}_{\pm} \simeq \dot{n}_{\pm} \mathcal{L}^3 \simeq \mathcal{B} \left(\frac{\sigma_T L_{\odot}^2}{m_e^2 G M_8 c^3} \right) l_X^2 e^{9.26\alpha} m_8^{-1} \quad (25)$$

³ α is used to extrapolate the spectrum from keV to MeV energies. It can be evaluated from X-ray data but this can be inaccurate due to localized spectral features. It can be evaluated more accurately from millimeter/X-ray colors.

where $(\sigma_T L_\odot^2 / m_e^2 GM_8 c^3) = 10^{31} \text{ s}^{-1}$. The dependence on black hole mass changes between Equations (24) and (25) because $\mathcal{L} \propto m_8$.

5. Pair production in RIAF - numerical results

We now evaluate the pair production rate numerically, check whether it matches the expected scaling laws, and evaluate $f(r, \mu)$. To do this, we have run simulations with a range of M and \dot{M} , assuming that the models have equal ion and electron temperatures, $T_e = T_i$. A list of model parameters is given in Table 1.

5.1. Pair creation rate

5.1.1. Dependence on model parameters: \dot{m} , m

The \dot{n}_\pm in models A through H (see Table 1) is well fit by

$$\dot{n}_\pm(r, \mu) = 3 \times 10^{40} \dot{m}^{3+2n_{sc}} m_8^{-1} \times \left(\frac{r}{\mathcal{L}}\right)^{-6} e^{-\mu^2/(2\sigma_\pm^2)} \text{ cm}^{-3} \text{ s}^{-1}, \quad (26)$$

or $\mathcal{A} \simeq 3$ in equation (20). The constant in Equation 26 is derived from models with $T_i/T_e = 1$. The constant is sensitive to T_i/T_e ; for $T_i/T_e = 3$ it is 10^{-4} times smaller. As expected, $\dot{n}_\pm \sim r^{-6}$ at large r ; surprisingly, however, this is also good fit at all r .

The pair production scale height $\sigma_\pm \approx 0.3$ independent of \dot{m} , m . This is nearly identical to σ_ρ , the plasma scale height. Notice that σ_\pm also controls f_{jet} the fraction produced inside the funnel. The funnel wall is at

$$\mu^2 > \mu_f^2 \approx \frac{r + 0.4GM/c^2}{r + 4GM/c^2}. \quad (27)$$

and $f_{jet} \approx 10\%$. Figure 5 shows a 2D contour map of \dot{n}_\pm corresponding to model C and Equation (26), and a contour marking the approximate funnel boundary. The grid averaged fractional difference between time averaged MHD models A through H and Equation (26) is $< 60\%$. Since \dot{n}_\pm is a steeply declining function of μ^2 , almost all free pairs are made near the funnel walls.

The pair production rate is well fit by

$$\dot{N}_\pm = 4 \times 10^{80} \dot{m}^{3+2n_{sc}} m_8^2 \text{ s}^{-1} \quad (28)$$

where a fit gives

$$n_{sc} = 1 + 0.03 \ln(m_8/\dot{m}). \quad (29)$$

Figure 6 compares the time-averaged numerical \dot{N}_\pm to Equation 28.

5.1.2. Dependence on l_X , α , m

The self-consistent radiative model enables us to calculate the emergent spectrum, from which we can measure a 2–10keV luminosity l_X and a spectral slope α . The pair production rate density can be measured in the same models. The numerical results are well fit by

$$\dot{n}_\pm(r, \mu) = 10^{-8} l_X^2 e^{9.26\alpha} m_8^{-4} \times \left(\frac{r}{\mathcal{L}}\right)^{-6} e^{-\mu^2/2\sigma_\pm^2} \text{ cm}^{-3} \text{ s}^{-1}. \quad (30)$$

or $\mathcal{B} \simeq 1$ in Equation (24). The fractional error of the fit is $< 50\%$ for time averaged models A-L.

The pair creation rate is well fit by

$$\dot{N}_\pm = 5 \times 10^{30} l_X^2 e^{9.26\alpha} m_8^{-1} \text{ s}^{-1} \quad (31)$$

Figure 7 compares \dot{N}_\pm to the semianalytic formula given by Equation 31 for different snapshots of the simulations with different mass accretion rates (models A-C) and black hole masses (models F-H). The semianalytic and numerical results agree well, and the scaling constants are close to those estimated in §4.

Although Equations (30) and (31) are strictly valid only for radiatively inefficient flows with $\dot{m} < \dot{m}_{crit}$, they depend mainly on the geometry of the radiation field and not on the radiative efficiency of the flow. We speculate that they provide a good estimate of the pair production rate even in more efficient systems, if σ_\pm is set to the scale height of the Comptonizing corona and the spectrum extends to sufficiently high energy.

5.2. Pair power and electromagnetic luminosity of a funnel

We define the funnel pair creation “luminosity”

$$L_\pm \equiv f_{jet} \dot{N}_\pm 2m_e c^2 \Gamma_{jet} \quad (32)$$

where Γ_{jet} is the jet bulk Lorentz factor at large r (assuming cold flow). Then

$$L_\pm \simeq 6 \times 10^{74} f_{jet} \dot{m}^{3+2n_{sc}} m_8^2 \Gamma_{jet} \text{ ergs s}^{-1} \quad (33)$$

and

$$L_\pm \simeq 10^{25} f_{jet} l_X^2 e^{9.26\alpha} m_8^{-1} \Gamma_{jet} \text{ ergs s}^{-1}. \quad (34)$$

It is interesting to compare this with the Blandford-Znajek (BZ), or electromagnetic, luminosity of the funnel

$$L_{BZ} = 2\pi \int_{\mu^2 > \mu_f^2} d\theta \sqrt{-g} T_t^r \quad (35)$$

where $T_t^r = b^2 u^r u_t - b^r b_t$ is the electromagnetic part of the stress-energy tensor and is computed directly from the simulation data. The BZ luminosity is well fit by

$$L_{BZ} \approx 8 \times 10^{45} (1 - \sqrt{1 - a_*^2})^2 \dot{m} m_8 \text{ ergs s}^{-1} \quad (36)$$

The scaling with a_* is taken from Equation (61) of McKinney & Gammie 2004, which is a fit to numerical data.

For mass comparable to that of Sgr A* and $a_* = 0.94$, $L_{BZ} > L_{\pm}/\Gamma_{jet}$ for $\dot{m} < \dot{m}_{crit} \approx 10^{-6}$ (for \dot{m}_{crit} see § 6.1). At low accretion rates the BZ luminosity completely dominates the pair luminosity, because the pair luminosity is such a steep function of accretion rate. Because $L_{\pm} \sim m_8^2$ while $L_{BZ} \sim m_8$, the \dot{m} at which $L_{BZ} \sim L_{\pm}$ is higher for lower mass black holes. L_{\pm}/L_{BZ} ratio is shown in the Table 1. For reasonable Γ_{jet} the funnel luminosity is therefore electromagnetically dominated for radiatively inefficient flows.

5.3. Energy-momentum deposition

Some of the pairs created in the funnel will escape to large radius and some will fall into the black hole. In an MHD model, the escaping fraction and asymptotic Lorentz factor will depend on the run of pair creation rate with radius, the magnetic field structure, the energy density of the pair plasma, and the pair-creation four-force G^μ .

Based on numerical calculations the spatial distribution of G^μ is well fit, with $x \equiv r/\mathcal{L}$, by

$$G_{code}^0(r, \mu) = G^0 \frac{\mathcal{L}^2 \mathcal{T}^2}{\mathcal{M}} \approx \frac{300}{x} \frac{\dot{n}_{\pm}(x, \mu) m_e c}{\mathcal{M}/(\mathcal{L}^2 \mathcal{T}^2)} \quad (37)$$

$$G_{code}^1(x, \mu) = G^1 \frac{\mathcal{L}^2 \mathcal{T}^2}{\mathcal{M}} \approx \frac{20(x - x_{st})}{x^2} \frac{\dot{n}_{\pm}(x, \mu) m_e c}{\mathcal{M}/(\mathcal{L}^2 \mathcal{T}^2)} \quad (38)$$

$$G_{code}^2(x, \mu) = G^2 \frac{\mathcal{L}^2 \mathcal{T}^2}{\mathcal{M}} \approx \frac{\mu}{x^2} \frac{\dot{n}_{\pm}(x, \mu) m_e c}{\mathcal{M}/(\mathcal{L}^2 \mathcal{T}^2)} \quad (39)$$

$$G_{code}^3(x, \mu) = G^3 \frac{\mathcal{L}^2 \mathcal{T}^2}{\mathcal{M}} \approx \frac{150}{x^2} \frac{\dot{n}_{\pm}(x, \mu) m_e c}{\mathcal{M}/(\mathcal{L}^2 \mathcal{T}^2)} \quad (40)$$

where \mathcal{M} , \mathcal{T} , \mathcal{L} , and \dot{n}_{\pm} are given in cgs units. The four-force vector components are given in a Kerr-Schild coordinate basis and in code units; we divide G^μ in cgs units by the unit of

the four-force density $\mathcal{M}/\mathcal{L}^2\mathcal{T}^2$. All components of the four-force depend more steeply on radius than \dot{n}_\pm . The radial component of the four-force is positive at large radius, zero at $x_{st} \approx x_{ISCO}(1+\mu^2/2)$, and negative at small radius. The sign of G^2 changes at the equatorial plane, as it should.

Pairs are created in the funnel with an initial distribution function, which is immediately isotropized with respect to rotation around the magnetic field. Later evolution of the distribution function depends on ill-understood relaxation processes; the pairs may not relax. Whether or not relaxation occurs the initial mean energy of the particles is of interest. So: what is $d\dot{n}_\pm/d\log\gamma_{e^\pm[FF]}$ (\equiv the energy distribution of newly created pairs), where $\gamma_{e^\pm[FF]}$ is the Lorentz factor of new particles measured in the fluid frame [FF]?

Four-momentum is conserved in pair creation, so the average Lorentz factor of the new leptons in the fluid frame is

$$\gamma_{e^\pm[FF]} = -\frac{1}{2}u_\mu(k^\mu + k'^\mu) \quad (41)$$

where u_μ is four-velocity of the background plasma and we assume that k^μ is in units of $m_e c^2$. Figure 8 shows $d\dot{n}_\pm/d\log\gamma_{e^\pm[FF]}$ in model C at $r = r_h, r_{isco}, 5GM/c^2$ (averaged over 20 radial zones from $\theta = 0 - 10$ deg; here $r_h \equiv$ event horizon radius). The distribution is flat and cuts off at $\gamma_{e^\pm[FF]max} \sim 100$ at $r = r_{isco}$.

If the thermalization timescale is short (which, given the low density and likely high temperature of the plasma, seems unlikely to us), then the rate of internal energy injection due to e^\pm creation is $\dot{u} = \dot{e}_\pm$, where the kinetic energy density injection rate, in the plasma frame, is ⁴

$$\dot{e}^\pm = \int d\gamma_{e^\pm[FF]} (\gamma_{e^\pm[FF]} - 1) m_e c^2 \frac{d\dot{n}_\pm}{d\gamma_{e^\pm[FF]}} \quad (42)$$

The corresponding temperature of the newly injected pairs is $\Theta_{e^\pm} = (1/3)\dot{e}_\pm/(\dot{n}_\pm m_e c^2) \approx (20, 10, 3)$ at $r = (r_h, r_{isco}, 5GM/c^2)$. This temperature is comparable to the thermal background plasma and is sub-virial. Pairs are not born hot.

The entropy of the injected pairs is likely to increase over the initial entropy. The funnel is exposed to “acoustic” radiation from the accretion disk. A small fraction of the MHD waves generated by turbulence in the disk will propagate toward the funnel, be transmitted at the funnel wall, and dissipate within the funnel. Because the density of the funnel is so low, even a small fraction of the disk acoustic luminosity is capable of raising the pair plasma temperature to $\Theta_e \gg 1$ before it can escape at Lorentz factor $\Gamma_{jet} \gg 1$. Until the magnitude

⁴ \dot{e}_\pm can be obtained by transforming G^μ from coordinate to fluid frame and subtracting the rest mass energy.

of turbulent heating can be estimated, the dynamics of the funnel pair plasma is extremely uncertain.

5.4. Comparison to Goldreich-Julian density

Pairs are created and then are accreted or escape on the light-crossing time \mathcal{T} . This implies a density $n_{\pm} \sim \dot{n}_{\pm} \mathcal{T}$ in the funnel. Is n_{\pm} sufficient to enforce the ideal MHD condition $\mathbf{E} = 0$ in the rest frame of the plasma ($u_{\mu} F^{\mu\nu} = 0$): does the pair number density exceed the Goldreich-Julian density n_{GJ} ?

A naive estimate of n_{GJ} uses the flat-space Goldreich-Julian charge number density

$$n_{GJ} \simeq \frac{\Omega B}{4\pi e c} = \frac{a_* B c^2}{32\pi G M e} \quad (43)$$

where the field rotation frequency in the funnel $\Omega = (a_*/8)c^3/(GM)$ in the Blandford-Znajek model at $a_* \lesssim 1$. For our standard Sgr A* model with $B \sim 30\text{G}$, $a_* \simeq 0.94$, $M \simeq 4.5 \times 10^6 M_{\odot}$, so $n_{GJ} \simeq 10^{-3} \text{cm}^{-3}$.

A better estimate uses the Blandford-Znajek model for a monopole magnetosphere. We use Kerr-Schild coordinates (t, r, θ, ϕ) and define the Goldreich-Julian density as the charge density measured in the frame of the normal observer, who to lowest (zeroth) order in a_* has four-velocity $n_{\mu} = (-(1 + 2/r)^{-1/2}, 0, 0, 0)$. Using the current density J^{μ} derived from the BZ monopole solution as given in McKinney & Gammie (2004) we find, to lowest order in a_* ,

$$n'_{GJ} \equiv -n_{\mu} J^{\mu} = \frac{a_* B^r c^2}{4\pi G M e} \frac{(1 + 2/x)^{1/2} \cos \theta}{x^3} \quad (44)$$

where $x \equiv r/\mathcal{L}$ and B^r is the radial component of the field at $x = 1$. This is close to the naive estimate.⁵ Notice that $n'_{GJ} \sim 1/r^3$, so n_{\pm}/n_{GJ} is smallest closest to the horizon if $n_{\pm} \sim 1/r^2$ as, for example, in a wind.

A still better estimate for n_{GJ} would use the simulation-derived currents. We have checked these and the charge densities are consistent with the estimates just given.

Using estimates for B^r from § 4, we can derive a scaling with \dot{m} and m :

$$n_{GJ} \sim 3 \times 10^{-1} a_* \dot{m}^{1/2} m_{\text{g}}^{-3/2} \text{cm}^{-3} \quad (45)$$

⁵Since $n'_{GJ} \sim B^r \cos \theta$ the charge density changes sign from one hemisphere to the other. In a split monopole model the sign would be the same.

near $x = 2$. Then using $n_{\pm} \sim \dot{n}_{\pm} \mathcal{T} \approx 5 \times 10^{40} \dot{m}^6$ (using Equation 26 and $\mu^2 = 1$):

$$\frac{n_{GJ}}{n_{\pm}} \sim 6 \times 10^{-42} a_* \dot{m}^{-11/2} m_8^{-3/2}. \quad (46)$$

This is the ratio at the axis. Although the Goldreich-Julian density varies only weakly across the funnel, $\dot{n}_{\pm}(\mu^2 = \mu_f^2)/\dot{n}_{\pm}(\mu^2 = 1) \simeq 20$ at $x \sim 2$. At very low \dot{m} , where $n_{GJ} \sim n_{\pm}$, the center of the funnel is populated by some other process—perhaps a pair cascade—and the edges by pair production in $\gamma\gamma$ collisions.

6. Discussion

6.1. Selfconsistency of the models

Our models are self-consistent when they are radiatively inefficient and n_{\pm} is greater than the Goldreich-Julian density. Figure 9 shows the self-consistent \dot{m}, M as a shaded region. The region is bounded at low accretion rates by the solid line, where $n_{\pm} = n_{GJ}$ (for $a_* = 0.94$). The region is bounded at high accretion rates by $\dot{m} = \dot{m}_{crit}$ (vertical dashed line), where the model becomes radiatively efficient (here defined as $L_{Bol}/\dot{M}c^2 = 0.1$). Numerically, $\dot{m}_{crit} \approx 10^{-6}$ at $T_i/T_e = 1$. The models are fully self-consistent in the resulting wedge in parameter space. They are never applicable to stellar mass black holes, which cannot produce enough pairs to exceed the Goldreich-Julian density even at \dot{m}_{crit} .

6.2. Sgr A*

The bright radio source associated with the $M = 4.5 \times 10^6 M_{\odot}$ black hole in the Galactic center, Sgr A*, is a weak X-ray source (‘quiescent’ emission $L_X \lesssim 10^{33} \text{ergs s}^{-1}$) and is strongly sub-Eddington ($L/L_{Edd} \approx 10^{-9}$). Mościbrodzka et al. (2009) have presented models of Sgr A* that suggest the most probable spin of the black hole $a_* = 0.94$, temperature ratio $T_i/T_e = 3$, and $\dot{m} = 2 \times 10^{-8}$. The \dot{n}_{\pm} rate for these parameters is lower than the scaling laws of §5 because $T_i/T_e > 1$. For the purposes of this subsection only we consider 3D GRMHD models that have \dot{n}_{\pm} very similar to the 2D models. All models assume the accretion flow lies in the equatorial plane of the black hole.

During the quiescent state the X-ray luminosity is $l_X < 1$. Near the horizon in the funnel, in model I, $\dot{n}_{\pm} \approx 10^{-9} \text{s}^{-1}$. The light crossing time is $\mathcal{T} \approx 20\text{s}$, so a typical pair density near the horizon in the funnel is $n_{\pm} \approx 10^{-8} \text{cm}^{-3}$. This is five orders of magnitude below $n_{GJ} \approx 10^{-3} \text{cm}^{-3}$. In quiescence the funnel must therefore (for the assumed spin) be

populated by a process other than $\gamma\gamma$ pair production process considered here, for example a pair cascade.

Sgr A* exhibits intraday variability at all observed wavelengths (radio, sub-mm, NIR, and X-rays). In particular in 2-10 keV luminosity may increase up to 160 times (the brightest flare detected has luminosity of $L_X = 5.4 \times 10^{34}$ Porquet et al. 2008) from the ‘quiescent’ level and last a few ks. During a bright flare the X-ray slope can change, and the implied pair density may reach or exceed n_{GJ} . Even during a flare the funnel kinetic luminosity is far below the Blandford-Znajek luminosity (see Table 1) for any reasonable Γ_{jet} . We conclude that close to the black hole any jet in Sgr A* is electromagnetically dominated.

6.3. M87

The core of M87 hosts a sub-Eddington black hole with $M = 3 \times 10^9 M_\odot$ (Marconi et al. 1997, but see Gebhardt & Thomas 2009) at distance $D \simeq 16$ Mpc. M87 has a prominent radio jet resolved from $100GM/c^2 - 1$ kpc. Reynolds et al. (1996b) have argued that models in which the jet is made of a pair plasma are favored over those in which the jet is composed of an ion-electron plasma. It is difficult to apply our model to M87 because the SED of M87 from $r < 100 GM/c^2$ includes contributions from both the accretion flow and the jet.

We assume $a_* = 0.94$, set the inclination $i = 30$ deg (Heinz & Begelman 1997), assume that the accretion disk lies in the equatorial plane of the black hole, that the electron distribution function is thermal, and that $T_i/T_e = 3$. The SED is normalized via $f_\nu(\nu = 230 \text{ GHz}) = 1770 \text{ mJy}$ at 16 Mpc (Tan et al. 2008). We find that the resulting zero cooling, 2D model with $\dot{m} = 1.5 \times 10^{-6}$ (model K) is radiatively efficient (see Table 1) and therefore not self-consistent.

To find a more self-consistent model we have run a GRMHD simulation with synchrotron and bremsstrahlung cooling, but not Compton cooling, included (model L, with $\dot{m} = 10^{-6}$). The cooling rates and cooling algorithm are presented in the Appendix. The efficiency is reduced to $\sim 30\%$. Figure 10 shows the SED for model L; the dotted line is the bremsstrahlung contribution, which is negligible. The model has $L_X = 10^{41} \text{ ergs s}^{-1}$, $L_\pm = 7 \times 10^{36} \text{ ergs s}^{-1}$, and $L_{BZ} \approx 10^{41} \text{ ergs s}^{-1}$.

If we identify L_{BZ} as the jet luminosity then the model is inconsistent with existing estimates (see the useful compilation of estimates in Table 3 of Li et al. (2009)), which range from $3 \times 10^{42} \text{ ergs s}^{-1}$ (Young et al. 2002) to $> 10^{44} \text{ ergs s}^{-1}$ estimated by Bicknell & Begelman (1996). The discrepancy between L_{BZ} in model L and observations is by 1-3 orders of magnitude, but the lowest ‘observed’ value of L_{BZ} could be possibly reached in a model

which combines $T_i/T_e \gtrsim 1$ and radiative cooling.

The jet is optically thin to pair annihilation: $\tau_{\pm} \approx n_{\pm} \mathcal{L} \sigma_T \approx 10^{-10}$. It is also optically thick to pair production for TeV photons, $\tau_{\gamma\gamma}(r) \sim \sigma_T n_{IR} \mathcal{L} \sim 10^3$, ($n_{IR} \approx 10^{13} \text{cm}^{-3}$ is the infrared photon density calculated from the Monte Carlo simulations).

The shape of the spatial distribution of pair production in model L is similar to that in models without cooling (although the scaling of the distribution changes). The implied pair density $n_{\pm} = \dot{n}_{\pm} \mathcal{T} \approx 10 \text{cm}^{-3}$ ($\mathcal{T} \approx 10^4 \text{s}$), which is 10^7 times larger than $n_{GJ} \approx 10^{-6} \text{cm}^{-3}$ in almost the entire computational domain.

Because of the shortcomings of the model, however, it is useful to use a more nearly model-independent estimate of the total pair production rate based on Equation (31). For $L_X \simeq 3 \times 10^{41}$ (7×10^{40} from Di Matteo et al. (2003) corrected upward to an isotropic X-ray luminosity because our models beam X-rays into the equatorial plane) and $\alpha_X = 0$, $\dot{N}_{\pm} \simeq 10^{45} \text{s}^{-1}$. This implies $L_K = f_{jet} \dot{N}_{\pm} m_e c^2 \Gamma_{jet} = 8 \times 10^{38} \Gamma_{jet} f_{jet}$. The implied pair density exceeds n_{GJ} for model L by $\sim 10^8$. Since $n_{GJ} \propto B \propto \dot{m}^{1/2}$ and $n_{\pm} \propto L_{512}^2$ the implied pair density will fall below the Goldreich-Julian density only for $(\dot{m}/10^{-6})^{1/2} (L_{512}/10^{41.5})^{-2} < 10^8$. Even if $\dot{m} \sim 10^{-4}$ this would require $L_{512} \sim 10^{38}$, which seems implausibly low given the $\sim 10^{40} \text{ergs s}^{-1}$ TeV luminosity (Aharonian et al. 2006). Therefore the main conclusion of this section does not change even if a more selfconsistent model is found.

There are significant limitations on the model. We have considered only one value of a_* ; estimates and preliminary models not described here show that the pair production rate is a steeply increasing function of a_* . Further preliminary models and a comparison of the $T_i/T_e = 3$ model for Sgr A* with the scaling relation for $T_i/T_e = 1$ models also show that the pair production rate declines sharply as T_i/T_e increases. But the allowed values of T_i/T_e are strongly constrained by submm VLBI (Fish & Doeleman 2010), because as T_i/T_e increases so does the size of the synchrotron photosphere.

After submission of this article Levinson & Rieger (2010) released a paper focused on modeling TeV emission and pair production in M87 (and Sgr A*). These authors use an ADAF model, assume that T_e saturates at $few \times 10^9 K$ ($\Theta_e \sim 1$), and set $\dot{m} \approx 10^{-4}$. The model is semi-analytic and does not include general relativistic effects. Bremsstrahlung is the dominant source of photons near the pair-production threshold, and the resulting radiation field is inadequate to raise the pair density above n_{GJ} . Levinson & Rieger (2010) therefore invoke a gap/pair cascade model to produce pairs.

We have investigated the Levinson & Rieger (2010) model by calculating images and an SED for a GRMHD/radiative transfer model with $\Theta_e = 1$ everywhere, $\dot{m} = 10^{-4}$, and $a_* = 0.94$. The model includes synchrotron, Compton and bremsstrahlung. We find $f_{230GHz} = 1 Jy$

(at $i = 30$ deg), and $L_{BZ} = 10^{43} \text{ergs s}^{-1}$, consistent with observations. Free-free cooling dominates over synchrotron cooling only at $r > 20 GM/c^2$. Levinson & Rieger neglect Compton cooling, but we find that Compton $y = A\tau \approx 12$ and that with Compton cooling included the model efficiency is $\approx 200\%$. The parameter space is large and the spectrum is parameter-sensitive, so there may be nearby models (with different a_* , Θ_e , \dot{m} , i) that are radiatively inefficient. The main point, however, is that self-consistent models can contain surprises that might not be anticipated in quasi-analytic estimates. Comptonization, in particular, occurs close to the innermost stable circular orbit, is therefore sensitive to the spin, and requires proper treatment of gravitational lensing. We concur with Levinson & Rieger’s conclusion that the pair production rate due to $\gamma\gamma$ collisions is small.

The model is also constrained by VLBI measurements. An optically thick spherical source of radius r and distance D in the Rayleigh-Jeans regime has flux $f_\nu \approx 2\pi\Theta_e m_e c^2 (r/D)^2 / \lambda^2$. Small r inferred from VLBI therefore requires high Θ_e . At 230 GHz (Fish & Doeleman 2010) report structure on scales of a “few Schwarzschild” radii, while we find the Levinson & Rieger model has a photosphere at $\approx 30 GM/c^2$. In comparison, our model L has a photosphere at $\sim 7 GM/c^2$. This argues against the Levinson & Rieger model if the reported structure arises from the accretion flow rather than the jet.

7. Summary

We have studied electron-positron pair production in black hole magnetospheres by $\gamma\gamma$ collisions. Our pair production rate simulations are based on a GRMHD time dependent model of a magnetized disk around a spinning black hole. The disk is a source of high energy radiation formed in multiple Compton scatterings of synchrotron photons. The pair production rates are calculated nearly *ab-initio* within $40 GM/c^2$ of the event horizon, using Monte Carlo methods.

The main results of this work are the fitting formulae for the rate and spatial distribution of pair production in terms of m_8 and \dot{m} (Equation [26]) and in terms of m_8 , L_X , and α (Equation [30]). These indicate that $\gamma\gamma$ pair production is concentrated close to the event horizon, and is sensitive to model parameters such as \dot{m} . The pair production rate is also sensitive to black hole spin a_* and the electron-ion temperature ratio T_i/T_e , but exploring the dependence on these parameters is beyond the scope of this paper.

We also find that the pair plasma is created with a power-law-like energy distribution. Most of the pairs are created in the equatorial plane of the thick disk because MeV photons created by Compton scattering are beamed into the equatorial plane. The pair plasma has

negligible effect on the accretion flow dynamical evolution, consistent with previous results by Esin 1999 and Kusunose & Mineshige 1996, assuming that it escapes on the viscous time scale.

Only a few percent of all pairs are created in the magnetized funnel (black hole magnetosphere), and most of pairs in the funnel are created near its wall. Pair jets will have spectra with a turnover frequency at around $\nu_t = 10^{-3}n_{\pm}\mathcal{L}$ Hz (for example, for M87 $\mathcal{L} = 4 \times 10^{14}$, and $n_{\pm} = 10$, turnover frequency $\nu_t = 10^{12}$ Hz).

We also find that the general relativistic RIAF models are selfconsistent up to $\dot{m}_{crit} \approx 10^{-6}$, which is consistent with the $\dot{m}_{crit} = 5 \times 10^{-6}$ reported by Fragile & Meier 2009. For higher \dot{m} one must couple the radiative cooling and forces into the dynamical model.

Models with $\dot{m} < \dot{m}_{crit}$ have force-free, Thomson thin jets with the Blandford-Znajek luminosity much larger than pair kinetic luminosity. In models with very small \dot{m} , the pair plasma density in the funnel is below the Goldreich-Julian density n_{GJ} , suggesting that another process, such as a pair cascades, will operate and populate the funnel.

We have applied versions of our model to Sgr A* and to M87. These models suggest that $n_{\pm} > n_{GJ}$ in M87 and $n_{\pm} < n_{GJ}$ in Sgr A*, with the important caveat that there are parameters (a_* and T_i/T_e) that we have not varied, and effects (Compton cooling, and nonthermal electrons) that we have not included.

REFERENCES

- Aharonian, F., Akhperjanian, A. G., Bazer-Bachi, A. R., Beilicke, M., Benbow, W., Berge, D., Bernlöhner, K., Boisson, C., Bolz, O., Borrel, V., Braun, I., Brown, A. M., Bühler, R., Büsching, I., Carrigan, S., Chadwick, P. M., Chounet, L., Coignet, G., Cornils, R., Costamante, L., Degrange, B., Dickinson, H. J., Djannati-Ataï, A., Drury, L. O., Dubus, G., Egberts, K., Emmanoulopoulos, D., Espigat, P., Feinstein, F., Ferrero, E., Fiasson, A., Fontaine, G., Funk, S., Funk, S., Füßling, M., Gallant, Y. A., Giebels, B., Glicenstein, J. F., Goret, P., Hadjichristidis, C., Hauser, D., Hauser, M., Heinzlmann, G., Henri, G., Hermann, G., Hinton, J. A., Hoffmann, A., Hofmann, W., Holleran, M., Hoppe, S., Horns, D., Jacholkowska, A., de Jager, O. C., Kendziorra, E., Kerschhaggl, M., Khélifi, B., Komin, N., Konopelko, A., Kosack, K., Lamanna, G., Latham, I. J., Le Gallou, R., Lemièrre, A., Lemoine-Goumard, M., Lenain, J., Lohse, T., Martin, J. M., Martineau-Huynh, O., Marcowith, A., Masterson, C., Maurin, G., McComb, T. J. L., Moulin, E., de Naurois, M., Nedbal, D., Nolan, S. J., Noutsos, A., Orford, K. J., Osborne, J. L., Ouchrif, M., Panter, M., Pelletier, G., Pita, S., Pühlhofer, G., Punch,

- M., Ranchon, S., Raubenheimer, B. C., Raue, M., Rayner, S. M., Reimer, A., Ripken, J., Rob, L., Rolland, L., Rosier-Lees, S., Rowell, G., Sahakian, V., Santangelo, A., Saugé, L., Schlenker, S., Schlickeiser, R., Schröder, R., Schwanke, U., Schwarzburg, S., Schwemmer, S., Shalchi, A., Sol, H., Spangler, D., Spanier, F., Steenkamp, R., Stegmann, C., Superina, G., Tam, P. H., Tavernet, J., Terrier, R., Tluczykont, M., van Eldik, C., Vasileiadis, G., Venter, C., Vialle, J. P., Vincent, P., Völk, H. J., Wagner, S. J., & Ward, M. 2006, *Science*, 314, 1424
- Alexanian, M. 1968, *Physical Review*, 165, 253
- Beckwith, K., Hawley, J. F., & Krolik, J. H. 2008, *ApJ*, 678, 1180
- Beskin, V. S., Istomin, Y. N., & Par'ev, V. I. 1992, *AZh*, 69, 1258
- Bicknell, G. V. & Begelman, M. C. 1996, *ApJ*, 467, 597
- Blandford, R. D. & Znajek, R. L. 1977, *MNRAS*, 179, 433
- De Villiers, J., Hawley, J. F., & Krolik, J. H. 2003, *ApJ*, 599, 1238
- Di Matteo, T., Allen, S. W., Fabian, A. C., Wilson, A. S., & Young, A. J. 2003, *ApJ*, 582, 133
- Dolence, J. C., Gammie, C. F., Mościbrodzka, M., & Leung, P. K. 2009, *ApJS*, 184, 387
- Dolence, J. C., Gammie, C. F., & Shiokawa, H. 2010, *ApJ*, 1, 1
- Esin, A. A. 1999, *ApJ*, 517, 381
- Fish, V. & Doeleman, S. 2010, in *COSPAR, Plenary Meeting, Vol. 38, 38th COSPAR Scientific Assembly*, 2303
- Fishbone, L. G. & Moncrief, V. 1976, *ApJ*, 207, 962
- Fragile, P. C. & Meier, D. L. 2009, *ApJ*, 693, 771
- Gammie, C. F., McKinney, J. C., & Tóth, G. 2003, *ApJ*, 589, 444
- Gebhardt, K. & Thomas, J. 2009, *ApJ*, 700, 1690
- Goldreich, P. & Julian, W. H. 1969, *ApJ*, 157, 869
- Gould, R. J. 1980, *ApJ*, 238, 1026

- Harms, R. J., Ford, H. C., Tsvetanov, Z. I., Hartig, G. F., Dressel, L. L., Kriss, G. A., Bohlin, R., Davidsen, A. F., Margon, B., & Kochhar, A. K. 1994, *ApJ*, 435, L35
- Hawley, J. F. & Krolik, J. H. 2006, *ApJ*, 641, 103
- Heinz, S. & Begelman, M. C. 1997, *ApJ*, 490, 653
- Hirokuni, K. & Okamoto, I. 1998, *ApJ*, 497, 563
- Jauch, J. M. & Rohrlich, F. 1976, *The theory of photons and electrons. The relativistic quantum field theory of charged particles with spin one-half*, ed. Jauch, J. M. & Rohrlich, F.
- Johnson, B. M. & Quataert, E. 2007, *ApJ*, 660, 1273
- Komissarov, S. S. 2005, *MNRAS*, 359, 801
- Krolik, J. H. 1999, *Active galactic nuclei : from the central black hole to the galactic environment*, ed. Krolik, J. H.
- Kusunose, M. & Mineshige, S. 1996, *ApJ*, 468, 330
- Leung, P., Gammie, C. F., & Noble, S. 2010, *ApJ*, 1, 1
- Levinson, A. & Rieger, F. 2010, *ArXiv e-prints*
- Li, Y., Yuan, Y., Wang, J., Wang, J., & Zhang, S. 2009, *ApJ*, 699, 513
- Marconi, A., Axon, D. J., Macchetto, F. D., Capetti, A., Sparks, W. B., & Crane, P. 1997, *MNRAS*, 289, L21
- Maxon, S. 1972, *Phys. Rev. A*, 5, 1630
- McKinney, J. C. & Gammie, C. F. 2004, *ApJ*, 611, 977
- Mościbrodzka, M., Gammie, C. F., Dolence, J. C., Shiokawa, H., & Leung, P. K. 2009, *ApJ*, 706, 497
- Narayan, R. & Yi, I. 1994, *ApJ*, 428, L13
- Noble, S. C., Krolik, J. H., & Hawley, J. F. 2009, *ApJ*, 692, 411
- Perlman, E. S., Sparks, W. B., Radomski, J., Packham, C., Fisher, R. S., Piña, R., & Biretta, J. A. 2001, *ApJ*, 561, L51

- Phinney, E. S. 1983, PhD thesis, , Univ. Cambridge, (1983)
- Phinney, E. S. 1995, in Bulletin of the American Astronomical Society, Vol. 27, Bulletin of the American Astronomical Society, 1450
- Porquet, D., Grosso, N., Predehl, P., Hasinger, G., Yusef-Zadeh, F., Aschenbach, B., Trap, G., Melia, F., Warwick, R. S., Goldwurm, A., Bélanger, G., Tanaka, Y., Genzel, R., Dodds-Eden, K., Sakano, M., & Ferrando, P. 2008, *A&A*, 488, 549
- Reynolds, C. S., Di Matteo, T., Fabian, A. C., Hwang, U., & Canizares, C. R. 1996a, *MNRAS*, 283, L111
- Reynolds, C. S., Fabian, A. C., Celotti, A., & Rees, M. J. 1996b, *MNRAS*, 283, 873
- Rybicki, G. B. & Lightman, A. P. 1986, *Radiative Processes in Astrophysics*, ed. Rybicki, G. B. & Lightman, A. P.
- Sharma, P., Hammett, G. W., Quataert, E., & Stone, J. M. 2006, *ApJ*, 637, 952
- Stepney, S. & Guilbert, P. W. 1983, *MNRAS*, 204, 1269
- Svensson, R. 1982, *ApJ*, 258, 335
- Tan, J. C., Beuther, H., Walter, F., & Blackman, E. G. 2008, *ApJ*, 689, 775
- Vincent, S. & Lebohec, S. 2010, *MNRAS*, 1256
- Wardziński, G. & Zdziarski, A. A. 2000, *MNRAS*, 314, 183
- Young, A. J., Wilson, A. S., & Mundell, C. G. 2002, *ApJ*, 579, 560

A. Synchrotron cooling rates including radiation self-absorption

The synchrotron cooling rate for a single electron is

$$\eta^T = \frac{2e^4 B^2 (\gamma^2 - 1) \sin^2 \xi}{3m_e^2 c^3} \quad (\text{A1})$$

where ξ is the pitch angle between electron velocity and magnetic field (e.g. Rybicki & Lightman 1986). To obtain the total cooling rate from the thermal population of electrons we integrate Equation (A1) against the relativistic Maxwellian distribution:

$$\frac{dn_e}{d\gamma d\cos\xi} = \frac{n_e\gamma(\gamma^2 - 1)^{1/2}}{2\Theta_e K_2(1/\Theta_e)} \exp\left(-\frac{\gamma}{\Theta_e}\right) \quad (\text{A2})$$

The resulting integral over $\cos\xi$ and γ is:

$$\Lambda_S = \frac{4B^2 e^4 n_e \Theta_e K_3(1/\Theta_e)}{3c^3 m_e^2 K_2(1/\Theta_e)} \quad (\text{A3})$$

For $x \ll 1$, $K_n(x) \rightarrow \Gamma(n)/2(2/x)^n$, so for large Θ_e ,

$$\Lambda \rightarrow \frac{16B^2 e^4 n_e \Theta_e^2}{3c^3 m_e^2} \quad (\text{A4})$$

This agrees with expression 14 in Wardziński & Zdziarski (2000). For $x \gg 1$ ($\Theta_e \ll 1$), $K_n(x) \rightarrow (\pi/2x)^{1/2} e^{-x}$, and

$$\Lambda_S = \frac{4B^2 e^4 n_e \Theta_e}{3c^3 m_e^2} \quad (\text{A5})$$

The ratio of these two expressions is $4\Theta_e$; a reasonable approximation is

$$\Theta_e \frac{K_3(1/\Theta_e)}{K_2(1/\Theta_e)} \approx (\Theta_e^m + (2\Theta_e)^{2m})^{1/m} \quad (\text{A6})$$

where $m = 4/3$ gives at most 4% error.

To account for synchrotron selfabsorption, Λ_S is multiplied by a factor:

$$f \equiv \frac{1}{\Lambda_{Syn}} \int_0^\infty d\nu \int_0^\pi \sin\theta d\theta j_\nu \exp(-\tau(\nu, \theta)) \approx \frac{1}{\Lambda_{Syn}} \int_{\nu_{crit}}^\infty d\nu \int_0^\pi \sin\theta d\theta j_\nu \quad (\text{A7})$$

where j_ν is given by Equation (3), Λ_{Syn} is the first integral without optical depth factor, ν_{crit} is the frequency where selfabsorption becomes important. The critical frequency is calculated numerically from:

$$\kappa_\nu(\theta = \pi/2)R = 1 \quad (\text{A8})$$

where $\kappa_\nu = j_\nu/B_\nu$, B_ν is the Planck function and $R = 0.1\mathcal{L}$. We find that f is well approximated by

$$f = \frac{1}{2} \left(\exp\left(-\frac{X_{crit}}{82}\right) + \exp\left(-\frac{X_{crit}}{360}\right) \right) \quad (\text{A9})$$

where $X_{crit} = \nu_{crit}/\nu_s$. This fit gives error for f less than 1% up to $X_{crit} = 10^2$ and 5% error at $X_{crit} = 10^3$.

B. Free-free cooling

The electron-ion bremsstrahlung cooling rate is (Stepney & Guilbert 1983):

$$\Lambda_{ei} = n_e n_p \sigma_T c \alpha_f m_e c^2 \begin{cases} \frac{9\Theta_e}{2\pi} (\ln(2\Theta_e \exp(-\gamma_E)) + 0.42) + 1.5 & \Theta_e \geq 1; \\ 4 \left(\frac{2\Theta_e}{\pi^3}\right)^{0.5} (1 + 1.78\Theta_e^{1.34}) & \alpha_f^2 \ll \Theta_e < 1. \end{cases} \quad (\text{B1})$$

where $\gamma_E = 0.5772$ is Euler constant and α_f is the fine structure constant. The electron-electron bremsstrahlung cooling rate is (Svensson 1982)

$$\Lambda_{ee} = n_e^2 \sigma_T c \alpha_f m_e c^2 \begin{cases} \frac{12}{\pi} \Theta_e (\ln(2\Theta_e \exp(-\gamma_E)) + \frac{5}{4}) & \Theta_e \geq 1; \\ \frac{5}{6\pi^{1.5}} (44 - 3\pi^2) \Theta_e^{1.5} (1 + 1.1\Theta_e + \Theta_e^2 - 1.25\Theta_e^{2.5}) & \alpha_f^2 \ll \Theta_e < 1. \end{cases} \quad (\text{B2})$$

The cooling rates are in units of $\text{ergs}^{-1} \text{cm}^{-3}$, and are consistent within a factor of 2 with those provided by e.g. Maxon (1972) or Gould (1980). Selfabsorption for free-free emission is negligible. For $\Theta_e > 1$ the ratio of synchrotron to bremsstrahlung cooling rate is approximately $\Theta_e^2/\beta\alpha_f$. Synchrotron cooling dominates over the free-free emission in all of models considered here.

C. Radiative cooling in MHD code

Radiative cooling is governed by

$$\frac{du}{dt} = \frac{du}{d\tau} \frac{1}{u^t} = -\frac{\Lambda}{u^t}. \quad (\text{C1})$$

where u is the internal energy per unit proper volume, τ is the proper time, and u^t is the time component of the fluid four-velocity.

Numerically u is evolved in an operator-split fashion. After each fluid timestep Δt , u is evolved using the second order scheme $u_{n+1} = u_n \exp(-\Delta t/\tau_{cool,n+1/2})$ and $\tau_{cool} = u/\Lambda$.

The cooling rates are calculated in cgs units, and then $\Lambda_{code} = \Lambda_{cgs} \mathcal{L} \mathcal{T}^3 / \mathcal{M}$.

D. Bremsstrahlung emissivity in the radiative transfer calculations

The emissivity for e-i interactions is (Stepney & Guilbert 1983):

$$j_\nu^{ei} = \frac{dE}{dt dV d\nu d\Omega} = \frac{1}{4\pi} n_i c h \int_{1+\omega}^{\infty} \omega \frac{d\sigma}{d\omega} \beta n_e(\gamma) d\gamma \quad (\text{D1})$$

where $\omega = h\nu/m_e c^2$, $n_e(\gamma)$ is relativistic Maxwellian electron energy distribution and the cross-section for this reactions is in the ultra-relativistic limit (Jauch & Rohrlich 1976). The $1/4\pi$ factor gives emissivity per unit solid angle. The integral is computed numerically using Gauss quadratures. The integration of Equation (D1) over photon energies and solid angle gives the total e-i cooling rate, Λ_{ei} .

The emissivity for e-e emission is also from Stepney & Guilbert (1983),

$$j_\nu^{ee} = \frac{1}{4\pi} n_e^2 \sigma_T c h \alpha_f \Theta_e \exp(-x) G(x, \Theta_e) \quad (\text{D2})$$

where $x = (h\nu/m_e c^2)/\Theta_e$ and $G(x, \Theta_e)$ is given in Stepney & Guilbert (1983). This formula is accurate to 5% over $0.1 < \Theta_e < 2$.

For $\Theta_e < 0.1$ we use a quadrupole approximation (Maxon 1972):

$$j_\nu^{ee} = \frac{1}{4\pi} \frac{2}{\pi} n_e^2 \sigma_T c h \alpha_f B(x) \sqrt{\frac{2\Theta_e}{\pi}} \exp\left(-\frac{x}{2}\right) K_0\left(\frac{x}{2}\right) \quad (\text{D3})$$

where $B(x) = 0.85 + 1.35\sqrt{x} + 0.38x$ and K_0 is the modified Bessel function of the second kind.

For $\Theta_e > 2$ we use the ultra-relativistic approximation (Alexanian 1968, Maxon 1972):

$$j_\nu^{ee} = \frac{1}{4\pi} \frac{3}{4\pi} n_e^2 \sigma_T c h \alpha_f \exp(-x) \left\{ \frac{28}{3} + 2x + \frac{x^2}{2} + 2\left(\frac{8}{3} + \frac{4}{3}x + x^2\right) \right. \\ \left. \times \left[\lg\left(\frac{2kT_e}{m_e c^2}\right) - 0.5777 \right] - \exp(x) Ei(-x) \left(\frac{8}{3} - 43x + x^2\right) \right\} \quad (\text{D4})$$

Formulas D2, D3, D4 connect smoothly at $\Theta_e=0.1$ and 2. Bremsstrahlung for e-e interactions dominates over e-i ones for $\Theta_e > 1$. Integration of j_ν^{ee} over frequencies and solid angle gives the total cooling rate, Λ_{ee} .

For details of the radiative transfer scheme see Dolence et al. (2009); we sample the bremsstrahlung radiation field in the same way as for synchrotron radiation, except that bremsstrahlung is emitted isotropically in the fluid frame. For the range of parameters considered in this work, energy loss by free-free emission is small in comparison to synchrotron and Compton losses.

Table 1. List of GRMHD models.

ID	a_*	m_8	$\langle \dot{m} \rangle_t$	L_{Bol}/L_{Edd}	radiative efficiency	$L_{\pm}/(L_{BZ}\Gamma_j)$	note
A	0.94	4.5×10^{-2}	2×10^{-9}	10^{-11}	7×10^{-4}	10^{-17}	2D
B	0.94	4.5×10^{-2}	6×10^{-9}	10^{-10}	2×10^{-3}	10^{-15}	2D
C	0.94	4.5×10^{-2}	1×10^{-8}	4×10^{-10}	4×10^{-3}	10^{-13}	2D
D	0.94	4.5×10^{-2}	5×10^{-8}	2×10^{-8}	0.02	10^{-10}	2D
E	0.94	4.5×10^{-2}	1×10^{-7}	6×10^{-8}	0.04	10^{-8}	2D
F	0.94	4.5×10^{-3}	1×10^{-8}	5×10^{-10}	5×10^{-3}	10^{-14}	2D
G	0.94	4.5×10^{-1}	1×10^{-8}	4×10^{-10}	4×10^{-3}	10^{-12}	2D
H	0.94	4.5	1×10^{-8}	3×10^{-8}	3×10^{-3}	10^{-11}	2D
Sgr A*							
I	0.94	4.5×10^{-2}	2.7×10^{-8}	5×10^{-10}	2×10^{-3}	10^{-11}	3D-quiescent, $T_i/T_e = 3$
J	0.94	4.5×10^{-2}	5.3×10^{-8}	1×10^{-9}	3×10^{-3}	10^{-9}	3D-weak flare, $T_i/T_e = 3$
M87							
K	0.94	30	1.5×10^{-6}	3×10^{-4}	16.5	0.1	2D - w/o cooling
L	0.94	30	1×10^{-6}	3×10^{-6}	0.3	4×10^{-5}	2D - w/ cooling

Note. — From left to right columns are: model ID, dimensionless spin of the black hole, the black hole mass in units of M_{\odot} , the rest mass accretion rate through the black hole horizon in units of Eddington mass accretion rate ($\dot{M}_{Edd} = 2.22m_8 M_{\odot}\text{yr}^{-1}$) averaged over later times of the simulation ($\Delta t = 1500 - 2000\mathcal{T}$), the Eddington ratio L_{Bol}/L_{Edd} , the model radiative efficiency $\eta = L_{Bol}/\dot{M}c^2$ (L_{Bol} is the RIAF luminosity integrated over emitting angles and frequencies), ratio of Kinetic to electromagnetic luminosity, and comments on models. Models I & J correspond to Sgr A* while K&L model M87. Run L accounts for cooling terms in the dynamical solution so the pair production rate is reduced.

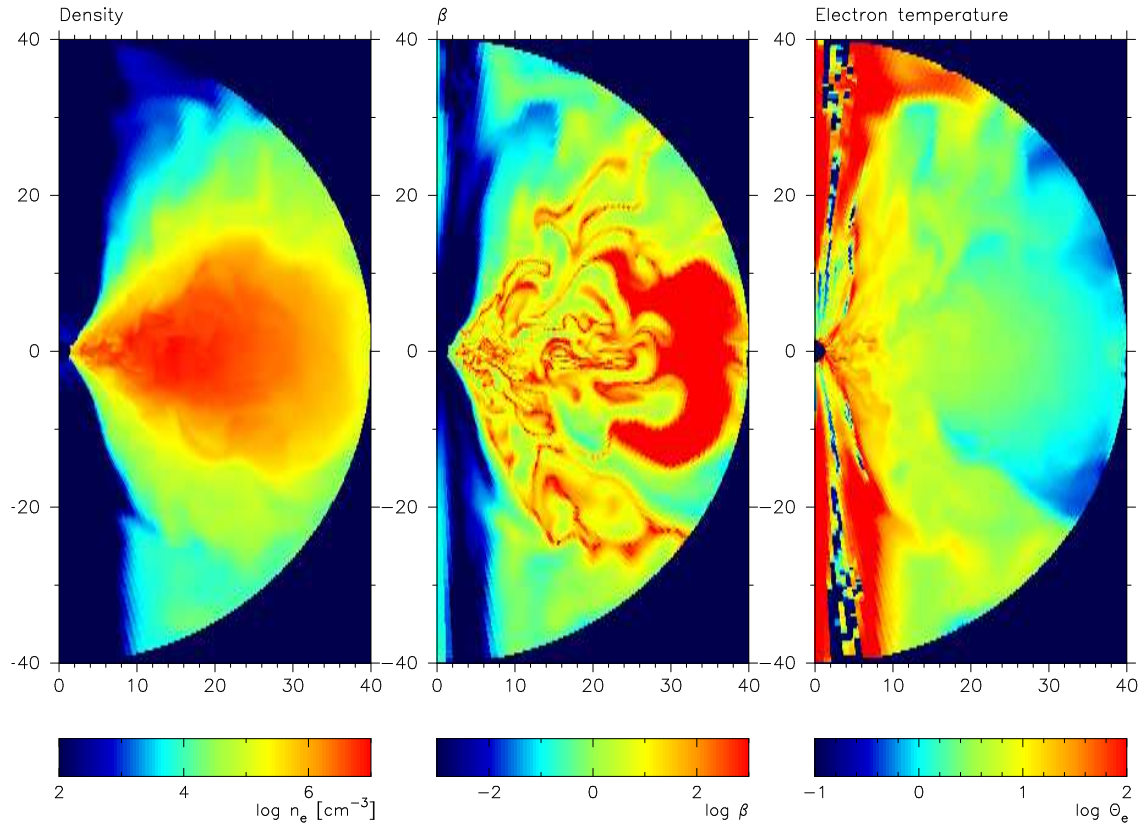


Fig. 1.— Structure of RIAF. Panels from left to right: density distribution, plasma β parameter, and dimensionless electron temperature, respectively.

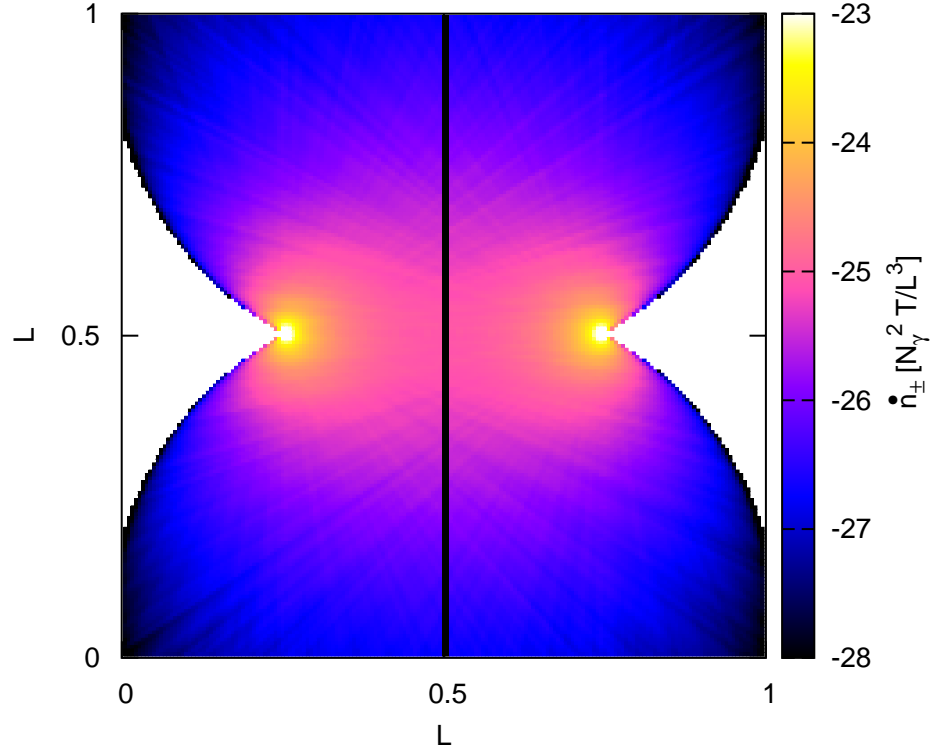


Fig. 2.— Test problem: the pair production rate in the plane of two, isotropic point sources of high energy radiation ($k_1^t = k_2^t = 4m_e c^2$). Pair production rate is given here in units of $\dot{N}_\gamma^2 T/L^3$, where L is a length unit, \dot{N}_γ is a number of photons produced by each source per unit time T . Pair production rate is zero in two side regions because the energy of photons in the center-of-momentum frame is below the threshold energy there. The pair production rate is symmetric with respect to the axis connecting two sources. Black contour - see Fig 3.

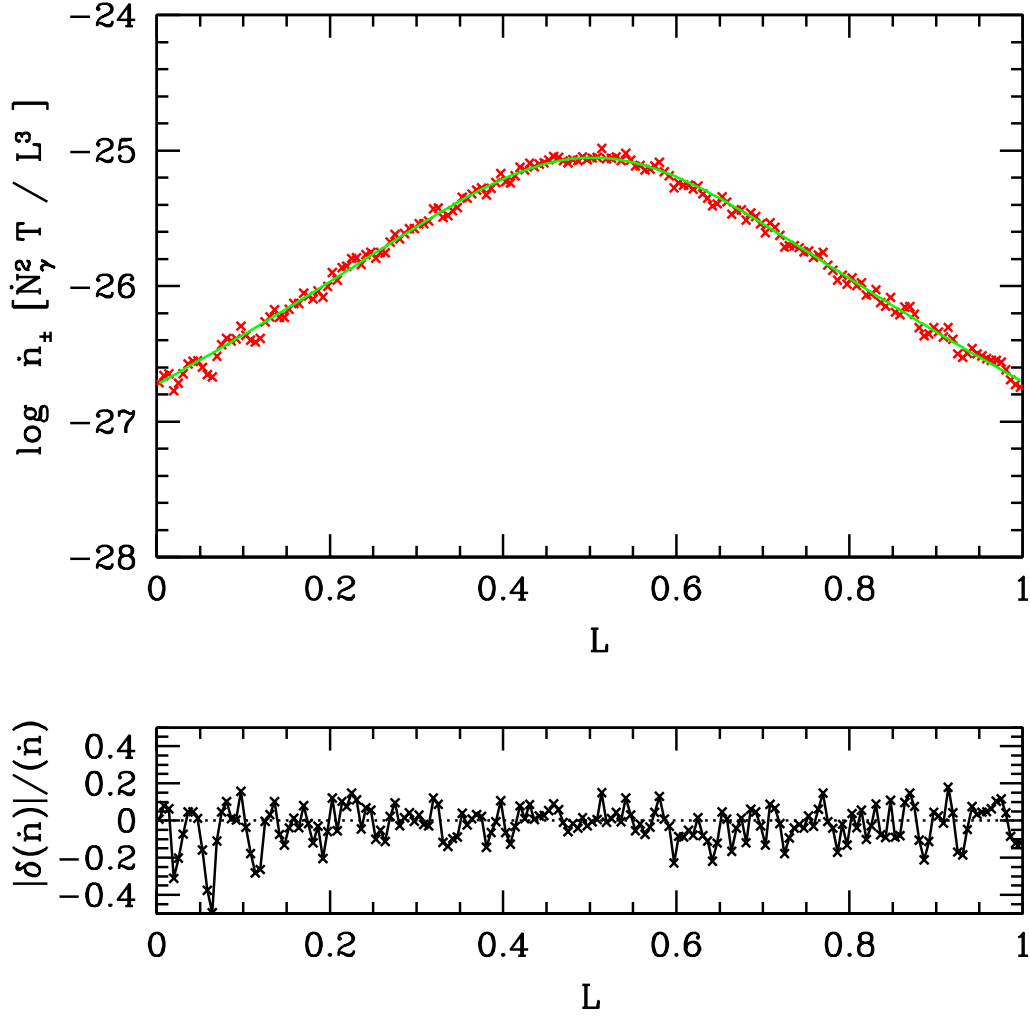


Fig. 3.— Test problem: upper panel: Analytical (green line) and numerical (red points) pair production rates, along the black contour in Figure 2. Lower panel: The fractional difference between analytical and numerical solutions.

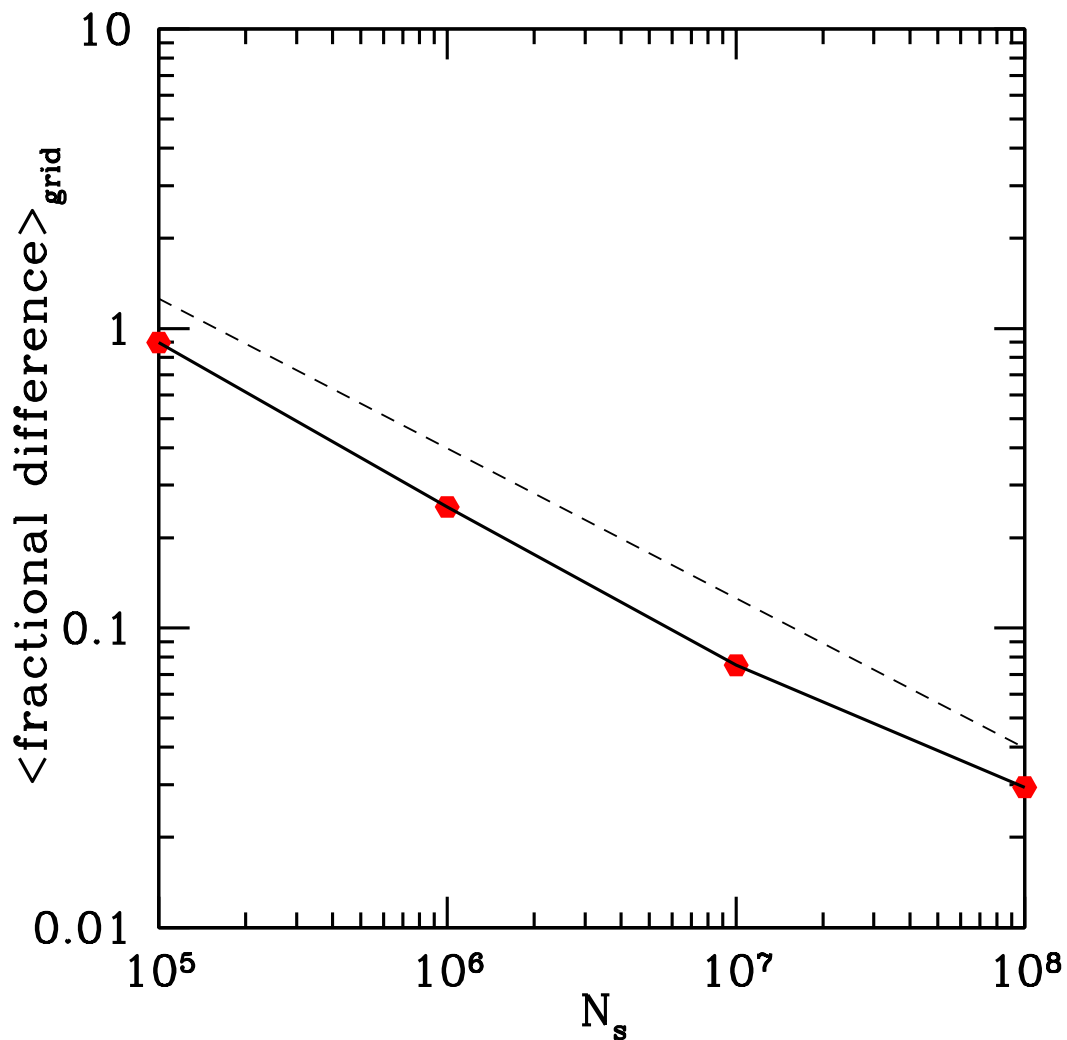


Fig. 4.— Test problem: the grid averaged fractional difference between the numerical and analytical pair production rates as a function of number of photons packets produced by each source N_s . The dashed line is proportional to $N_s^{-1/2}$. For $N_s = 10^7$ the average difference per zone is about 7%, for $N_s = 10^8$ it is on average less than 3%.

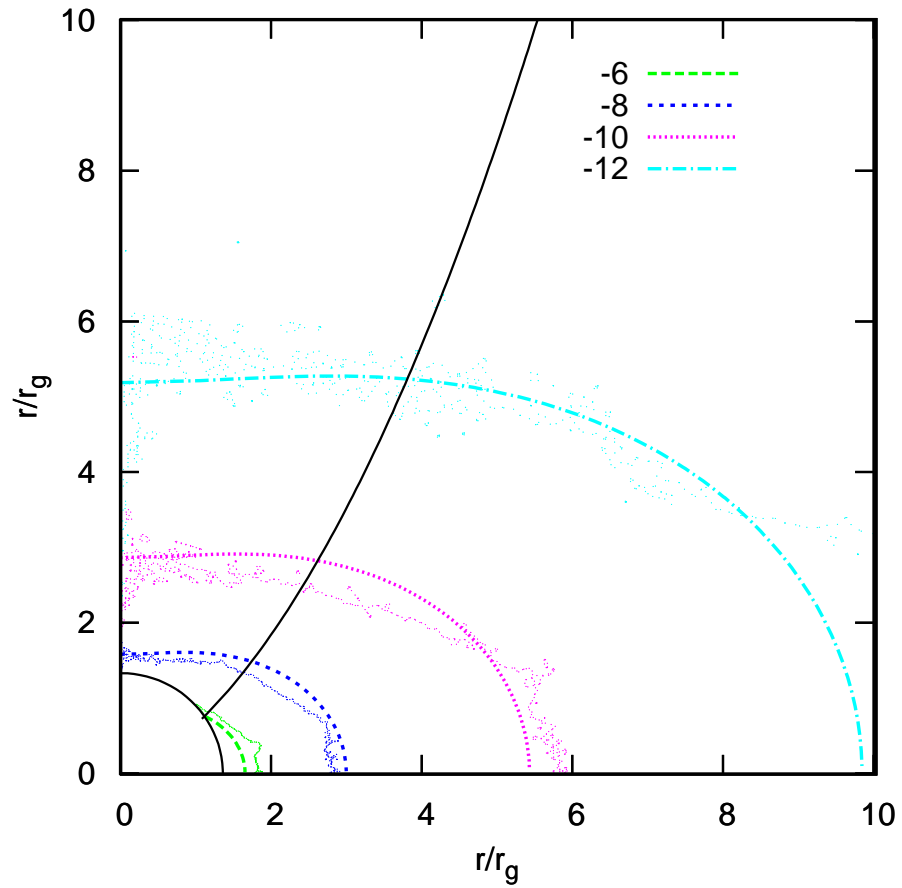


Fig. 5.— Spatial distribution of \dot{n}_{\pm} in RIAF model C (points) and the contours of corresponding fitting function given by Equation 26 (lines). The fractional difference between model and data in this case is $< 40\%$. Black contours mark the black hole horizon and the funnel wall.

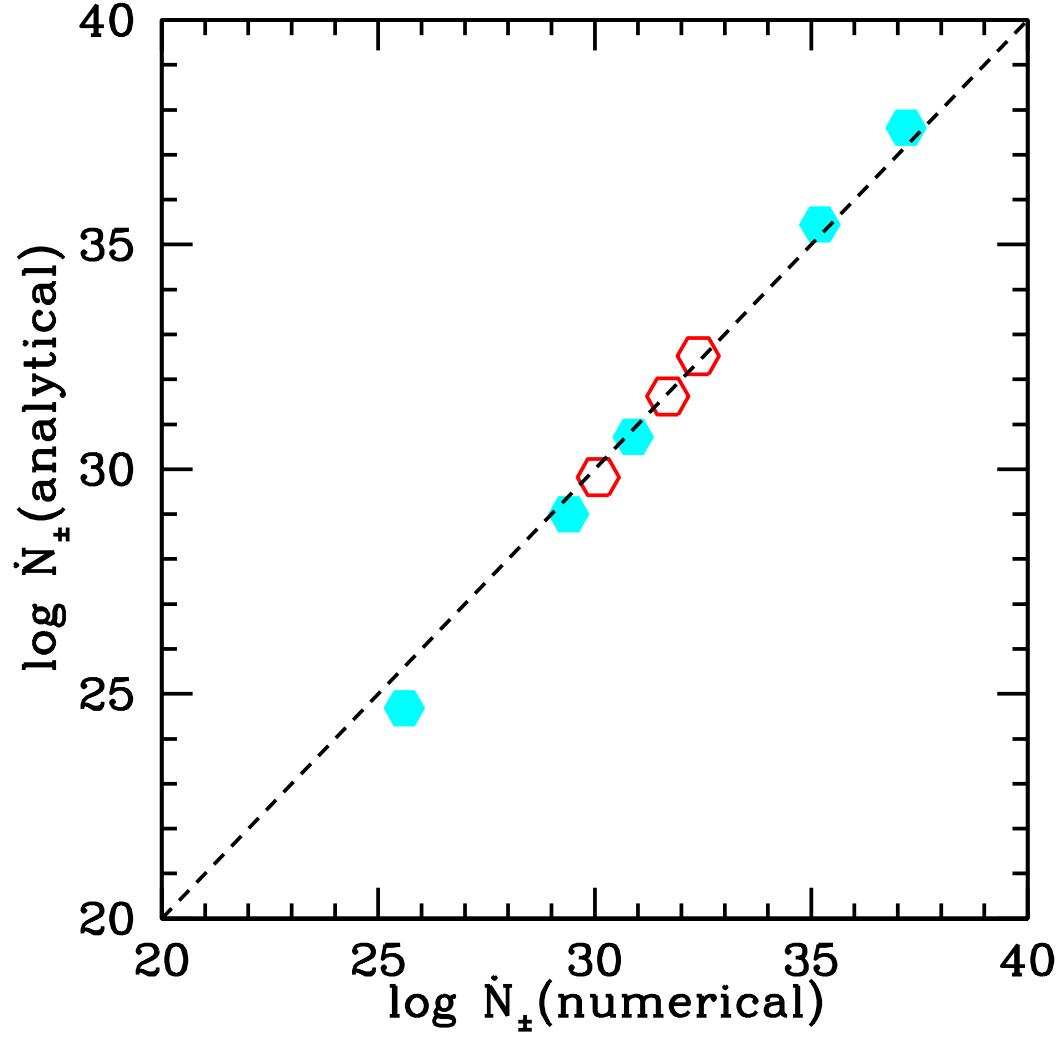


Fig. 6.— Pair production rate dependence on the model parameters. Comparison of the total pair production rate \dot{N}_{\pm} to the fitting formula for models with various mass accretion rates \dot{m} (A-E, blue filled symbols), and black hole masses m (F-H, red open symbols). The $\dot{N}_{\pm}(\text{analytical})$ is given by Equation 28.

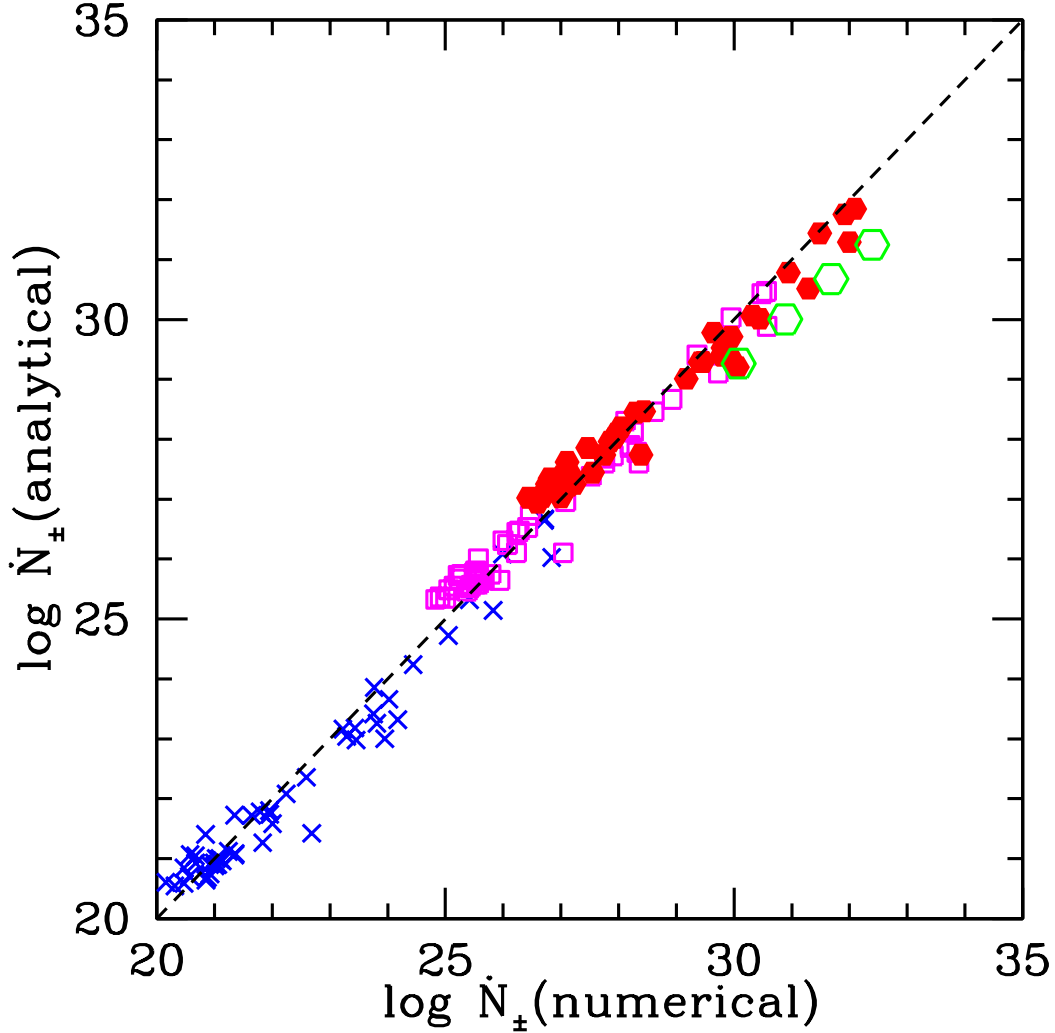


Fig. 7.— Pair production rate dependence on observable parameters. Comparison of the total pair production rate \dot{N}_{\pm} to the fitting formula for models with different X-ray luminosities $(\nu L_{\nu})_{2-10\text{keV}}$, X-ray spectral index α and masses. Crosses, open squares, filled circles correspond to different snapshots in models A, B, and C, respectively. Open circles mark time averaged data from models with different masses (F, G, and H). The $\dot{N}_{\pm}(\text{analytical})$ is given by Equation 31.

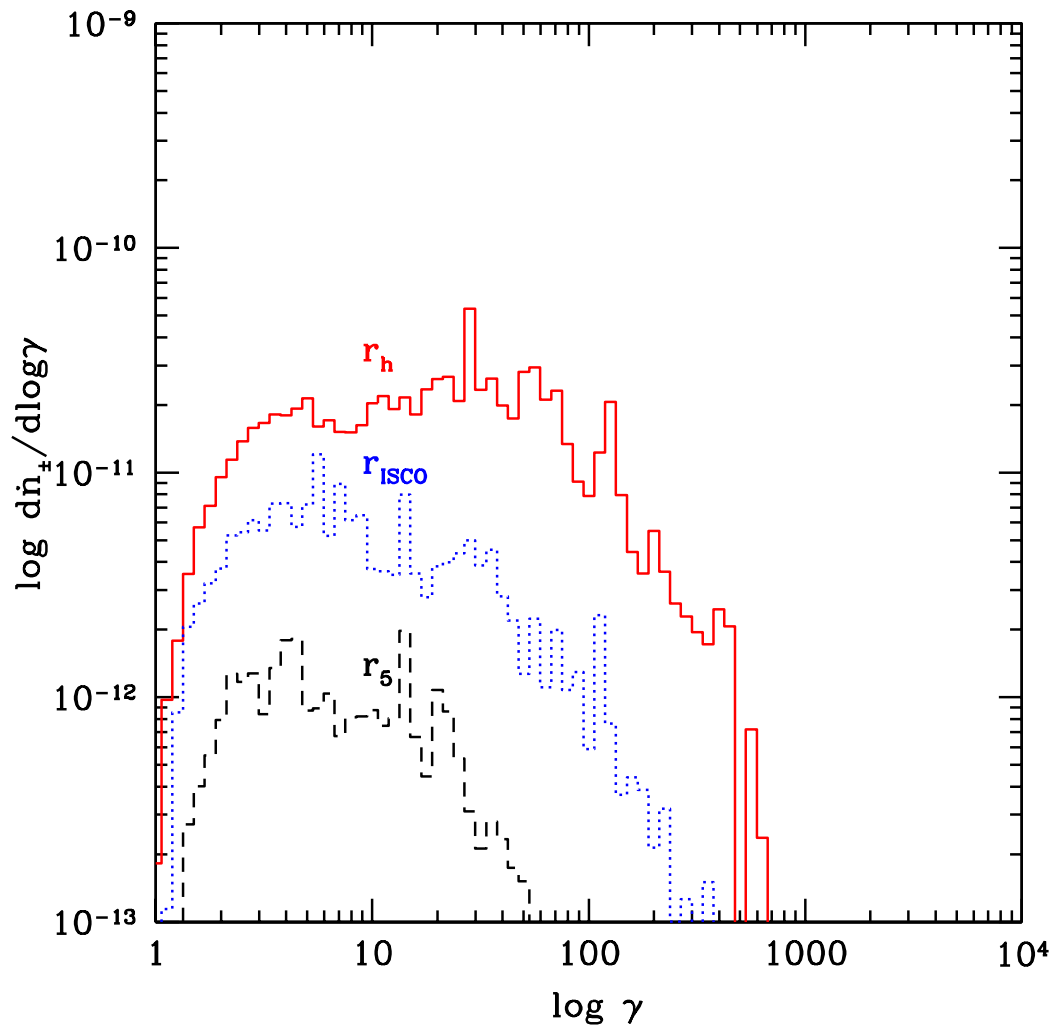


Fig. 8.— The energy distribution of e^\pm pairs produced in the magnetized funnel where $\gamma = \gamma_{e^\pm[FF]}$ is measured in the plasma frame at different radii (single time slice of model C).

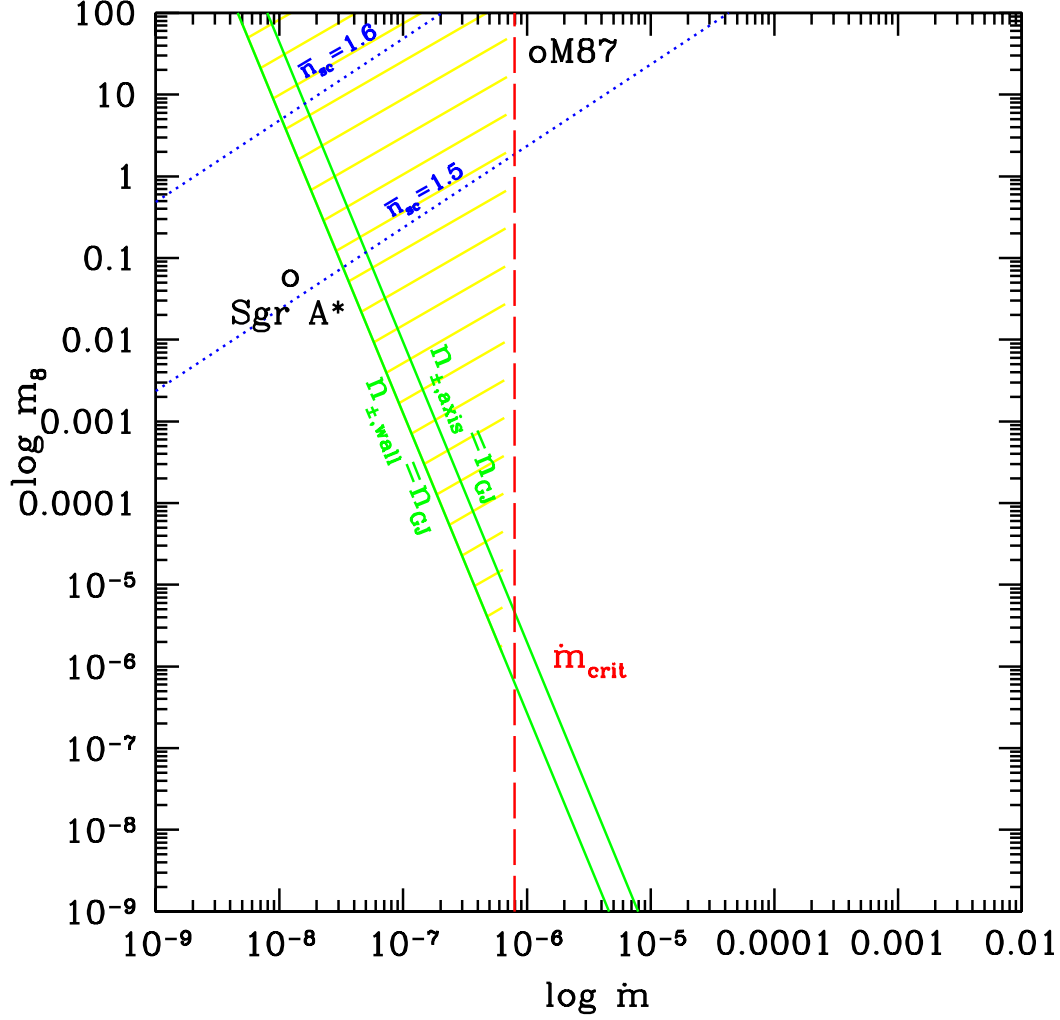


Fig. 9.— Fitting formulas are fully selfconsistent with the model assumptions for m and \dot{m} within the shaded region. Two solid lines mark regions where the n_{GJ} equals to the pair density at the funnel axis and funnel wall. Dotted lines shows scaling law for the number of scatterings (n_{sc}). Sgr A* and M87 are marked as open circles.

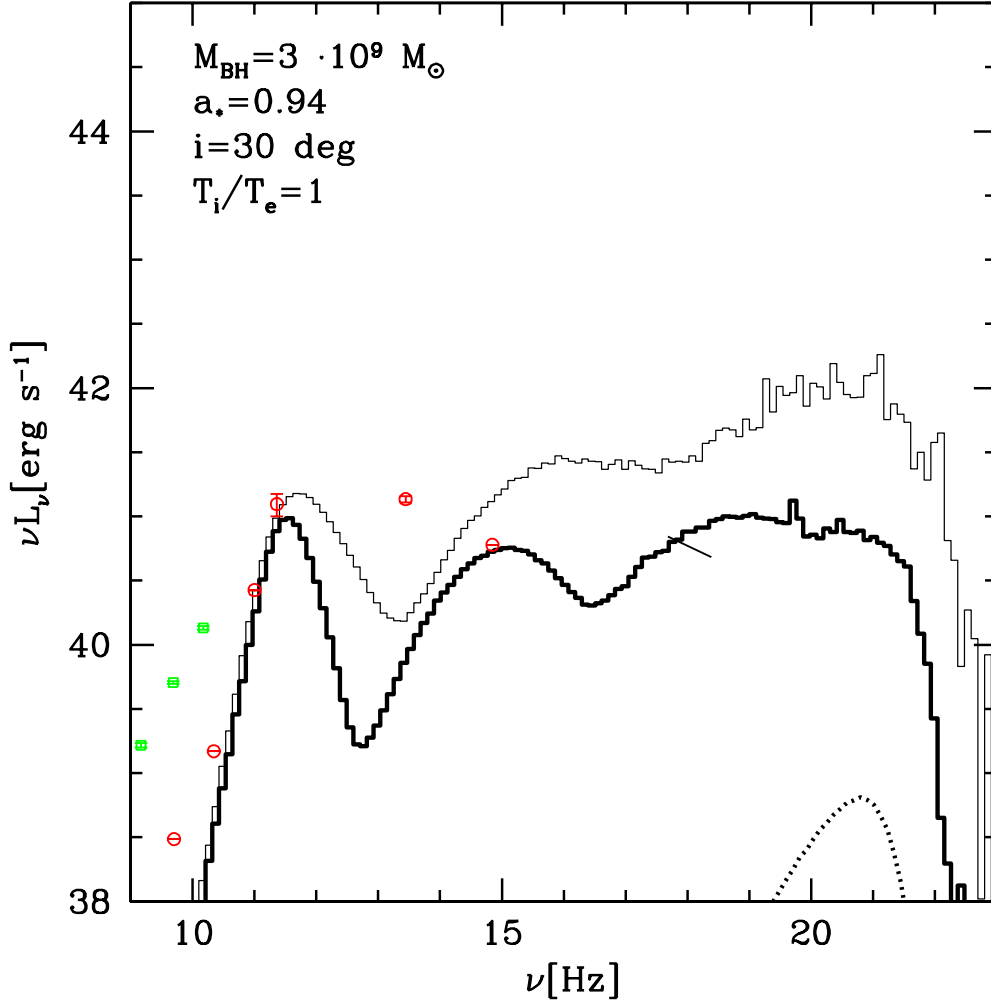


Fig. 10.— Model L: time averaged spectral energy distribution. Two lines show model with $\dot{m} = 10^{-6}$ and $T_i/T_e = 1$. \dot{m} is chosen to normalize to 1.7 Jy at 230 GHz. Thick-solid line corresponds to run in which a radiative cooling is taken into account as described in the Appendix. Dotted lines is a free-free process spectrum. Model, that does not accounts for any cooling in the MHD simulation, is marked as thin-solid line (also this model is not shown in the table). Observational points are taken from: Reynolds et al. (1996a), Tan et al. (2008) (230 GHz), Perlman et al. (2001) ($10.8 \mu m$), Harms et al. (1994) (7×10^{14} Hz) Di Matteo et al. (2003) (2-10 keV)